LINEAR ELECTROMAGNETIC ENERGY SCAVENGING DEVICE DESIGNED IN LOW TEMPERATURE CO-FIRED CERAMICS

by

Hope A Bateman

A thesis

submitted in partial fulfillment

of the requirements for the degree of

Master of Science in Mechanical Engineering

Boise State University

December 2011

BOISE STATE UNIVERSITY GRADUATE COLLEGE

DEFENSE COMMITTEE AND FINAL READING APPROVALS

of the thesis submitted by

Hope A Bateman

Thesis Title: Linear Electromagnetic Energy Scavenging Device Designed in Low Temperature Co-Fired Ceramics

Date of Final Oral Examination: 19 October 2011

The following individuals read and discussed the thesis submitted by student Hope A Bateman, and they evaluated her presentation and response to questions during the final oral examination. They found that the student passed the final oral examination.

Donald G Plumlee, Ph.D.	Chair, Supervisory Committee
John F Gardner, Ph.D.	Member, Supervisory Committee
Joseph Guarino, Ph.D.	Member, Supervisory Committee
Stephen Tennyson, Ph.D.	Member, Supervisory Committee

The final reading approval of the thesis was granted by Donald G Plumlee, Ph.D., Chair of the Supervisory Committee. The thesis was approved for the Graduate College by John R. Pelton, Ph.D., Dean of the Graduate College.

ABSTRACT

For a soldier deployed in a remote location on the earth or a recreational hiker in the wilderness or a wild land firefighter battling a destructive wildfire, access to a power source is problematic. Local and regional communication systems, navigation, lights, imaging: all of these require a power source. For short time periods, batteries may be sufficient but with extended time periods the weight of the batteries and cost of replacement becomes a problem. Energy scavenging devices could fill this need and be used as a secondary power source when solar or batteries are not available.

A linear electromagnetic generator is designed and prototyped for use in a frame backpack configuration. A base excitation vibration model is developed to predict the available energy from the movement of a person walking while wearing a backpack. The energy scavenging device takes the ambient movement of the person walking and converts it to usable energy. The electromagnetic generator does not affect how the person walks and will decrease the weight carried by a soldier or backpacker by replacing batteries. An analytic model of the mechanical and magnetic systems is developed to determine and optimize for the design parameters of the electromagnetic generator. The induction coils for the electromagnetic generator were fabricated in Low Temperature

Co-Fired Ceramics (LTCC), taking advantage of the material system to produce a small high density package of coils.

LTCC induction coils were found to be a viable way of scavenging energy. It was determined that the electromagnetic generator has the potential for producing the required energy need by a soldier or backpacker. Future work includes testing of the induction coils, and designing the frame of the backpack and energy storage of the electromagnetic generator.

TABLE OF CONTENTS

LIST OF TABLES

LIST OF FIGURES

LIST OF SYMBOLS

μ_r	relative permeability
ω_b	Base Frequency (radians/second)
ω_n	Natural Frequency (radians/second)
ϕ	Flux (Weber)
ξ	Damping Ratio
B_g	Flux Density at the Surface of the Rotor (Tesla)
B_r	Remnant Flux Density (Tesla)
B(R)	Flux Density across the Coil (Tesla)
c	Damping Coefficient (kilogram/second)
ch	Thickness of the Coil (meters)
cw	Coil Width (meters)
F_c	Force on the Coil (Newton)
F_{mag}	Magnetic Force on Coil (Newton)
gap	Air Gap between the Coil and Magnet (meters)
I_c	Induced Current (Amps)
J_c	Induced Current Density (Amps/ meters squared)

k	Spring Constant (Newton/meter)
l_g	Effective Air Gap (meters)
L_p	Pathlength of the Coil (meters)
m	Mass of Backpack (kilograms)
P_{rms}	RMS Power (Watts)
r	Frequency Ratio
R	Variable Radius (meters)
R_i	Inner Radius of Coil (meters)
R_m	Radius of the Magnet (meters)
R_o	Outer Radius of Coil (meters)
t	Time (seconds)
Δv	Relative Velocity (meters/second)
Δv_{rms}	RMS Relative Velocity (meters/second)
w_m	Width of the Magnet (meters)
w_s	Width of Steel Spacer (meters)
x	Position of Mass/ Backpack (meters)
X	Amplitude of Backpack (meters)
$\dot{x}$	Velocity of Backpack (meters/second)
$\ddot{x}$	Acceleration of Backpack (meters squared/ second)

y	Position of Base/ Person (meters)
$\dot{y}$	Velocity of Base (meters/second)
Y	Amplitude of Base (meters)

INTRODUCTION

Electronic advances have led to new devices with the following capabilities: warning soldiers of chemical or explosive hazards, maintaining communications lines between soldiers and aircraft, precision navigation on the battlefield, laser guidance systems, and night vision imagery as seen in Figure 1. This enhanced electronic capability has boosted the weight of a typical soldier's batteries to approximately 12 kilograms according to Patal-Predo [1]. This trend has been particularly significant over the last ten years and will continue in the future. Carrying an additional 12 kilogram battery pack is an additional burden for each soldier, but recharging or replacing these batteries in a remote battlefield is difficult logistically and very costly. The soldiers using these battery packs are located in remote areas at the limit of the military supply chain. An alternative power source that could reduce the battery weight and the frequency of battery replacement would improve the efficiency of individual soldiers and optimize the military supply chain.

Figure 1. Communications in the Modern Battlefield [2]

The modern backcountry hiker or backpacker has experienced an increase in available electronic tools and subsequent power requirements that is analogous to the increased load of the modern soldier. The modern hiker uses communication equipment such as a cell phone and two-way radios, navigation equipment such as a Global Position System (GPS), imagery equipment such as digital cameras, and various lighting devices. Each of these devices requires a battery pack that contributes additional weight and must be recharged after use.

The need for an individual power source falls in between the macro-scale generation of a Brayton cycle turbine and the micro-scale generation of a piezoelectric crystal, according to Dunn-Rankin et al. [3]. A chart comparing needed power with stored energy can be used to describe the energy requirements of various applications as shown in Figure 2. The personal power devices used in the field fall into the shaded area above a power of 10 W with a stored energy greater than 10 Whr. A high generation of power can be produced, but without a large energy, the devices using the power will not work for a long period of time. In comparison, the Ragone [4] chart comparing power density with energy density for a variety of power generation sources is shown in Figure 3. The combustion engine group clearly achieves the highest energy and power densities, but the technology for micro-combustion systems is currently under development and not available for implementation. Electromagnetic generation significantly outperforms photovoltaic cells and thermoelectric generation. Fuel cells are another area of research with potential for remote power. Based on this data, the individual power requirements fall into an area that is currently best served by batteries. A soldier on a 72-hour mission needs a reliable energy source that will provide at least 10 Watts and last for the duration of the mission, a breakdown of power requirements for a soldier is shown in Figure 4. This shows that the largest component of energy usage is the computer/radio system. Most soldiers do not carry a computer, but do carry everything else shown and from this the requirements of power generation needed by a soldier or backpacker were determined.

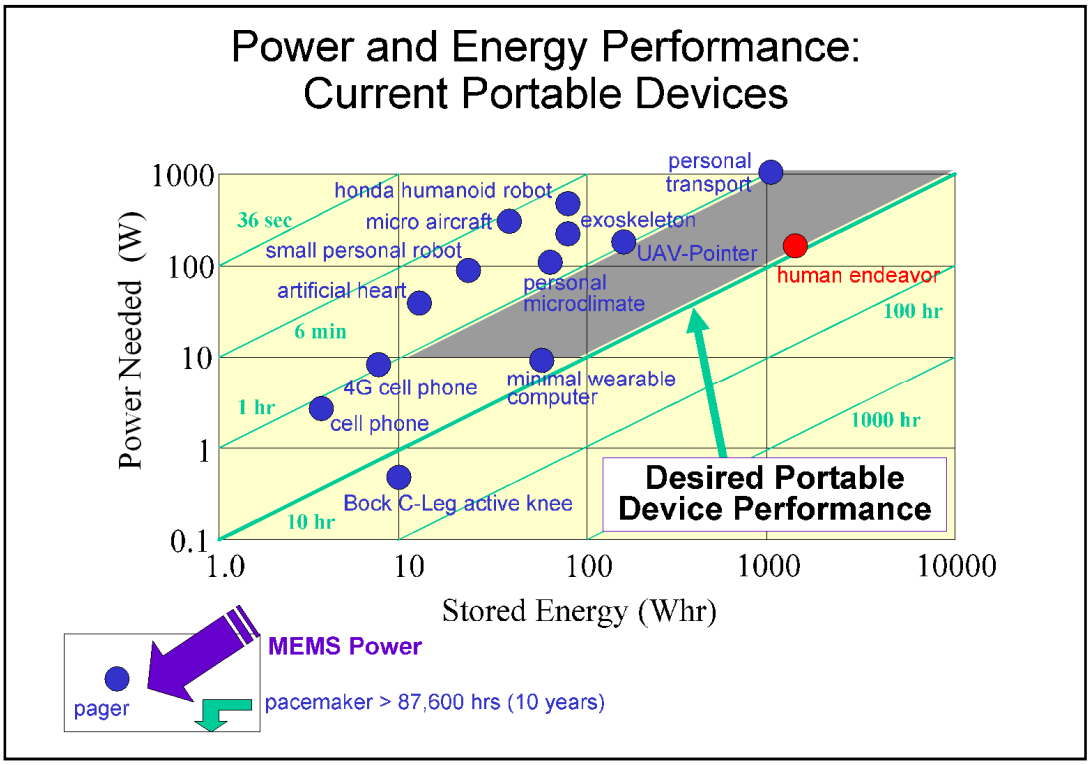

Figure 2. Power Requirements for Portable Devices [3]

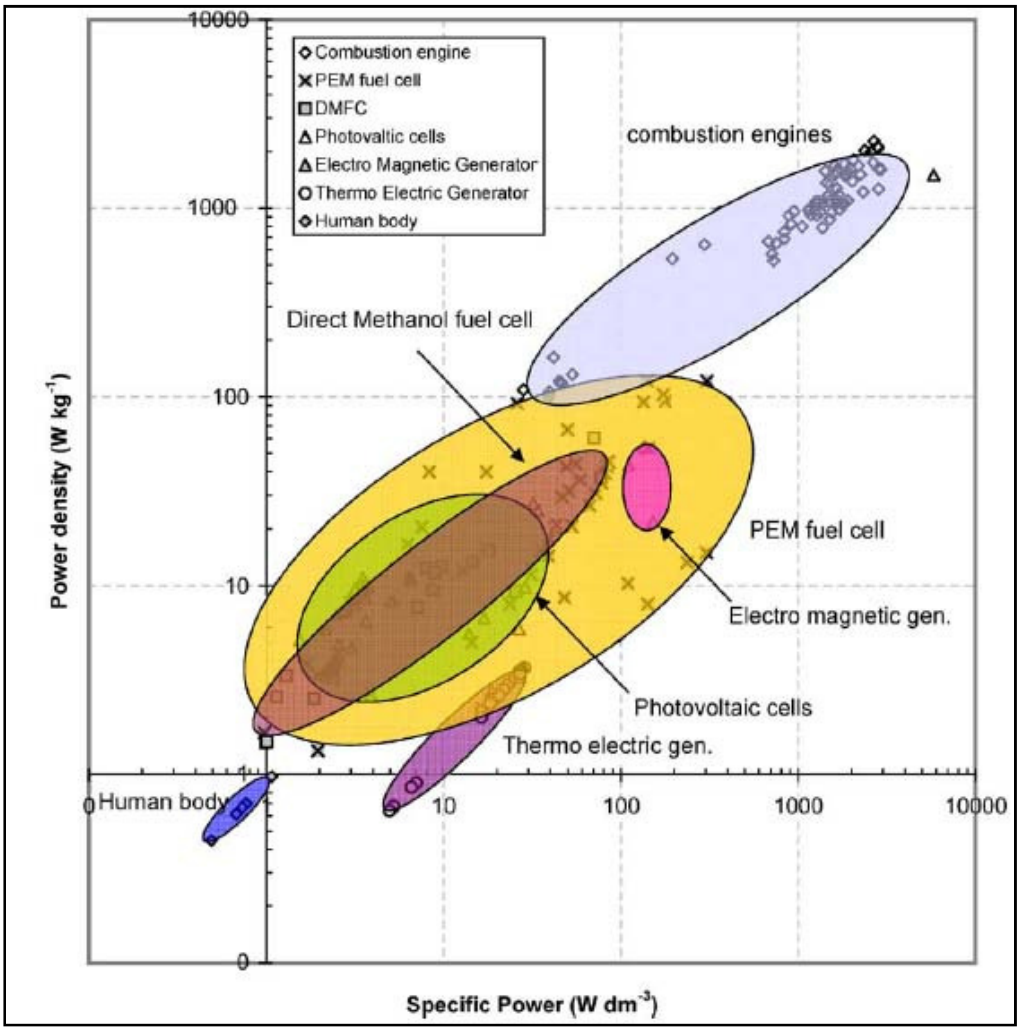

Figure 3. Power Sources Compared [4]

	Functional Operating Power (W)
Computer/Radio Subsystem	
Computer	14.800
Hand-Held Flat Panel Display	6.400
Soldier Radio	
Receive	1.400
Transmit	6.000
Squad Radio	
Receive	2.000
Transmit	12.000
Global Positioning System	1.500
Video Capture	1.000
Subtotal	45.100
Integrated Helmet and Sight Subsystem (IHAS)	
Laser Detectors	0.600
Helmet-Mounted Display	4.900
Imager	0.100
Subtotal	5.600
Weapon Subsystem	
Laser Rangefinder	0.050
Laser Aiming Light	0.075
Digital Compass	0.350
Thermal Weapon Sight	5.525
Subtotal	6.000
TOTAL	56.7

Figure 4. Power Requirements for the Land Warrior System [5]

The developments that led to the variety of electronic sensors and communication devices have not translated into the area of micro-power generation. Photovoltaic (PV) cells, micro-engines, and energy scavengers have been pursued to address the need for micro-power with limited success. However, for each of these technologies, technical and practical challenges have limited their full-scale adoption. Photovoltaic cells are well established but are inefficient, expensive, and are not effective at night, in the forest, or

on cloudy days. Micro-engines, such as the micro-wankel engine [6] shown in Figure 5, have the highest potential power density, but are limited by current fabrication capabilities used in the electronics industry. A wide variety of power scavengers have been developed that typically use piezoelectric materials or electromagnetic induction to generate power from ambient vibrations. Piezoelectric devices generate high output voltages but very little usable output power. Piezoelectric applications, such as the shoe power system shown in Figure 6, which produces 2mW, Shenck and Paradiso [7], are typical of Micro-Electrical Mechanical Systems (MEMS) energy devices, which produce a small amount of power compared to portable power requirements needed by soldiers and backpackers. MEMS fabrication methods draw from the vast processing knowledge of the semiconductor industry and piezoelectric power generation has significant advantages when scaled to the small Mirco-Electro-Mechanical Systems (MEMS) size range. Typical semiconductor processing is batch processing technology including photolithography and deep reactive ion etching (DRIE). Photolithography is the process of transferring a pattern onto thin film. DRIE uses a high-density plasma source to dry etch patterns according to Madou [8]. Batch processing works well for large production, but if production is limited the process becomes expensive. Several researchers have investigated MEMS devices fabricated in silicon to address the need for micro-power generation. Epstein and Senturia [9] are developing a micro-scale gas turbine generator device that combines a radial compressor and turbine with a catalytic combustor, seen in Figure 7, but the technical challenges of scaling down an effective macro-scale engine

have limited its capability. Also, this device would be unrealistic in the field because of the fuel requirements.

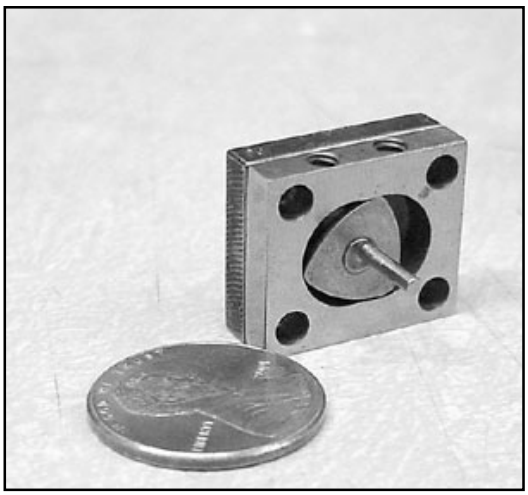

Figure 5. Micro-Wankel Designed by Engineers at UC Berkeley [6]

Figure 6. Power Generation Using a Piezoelectric Source in a Shoe [7]

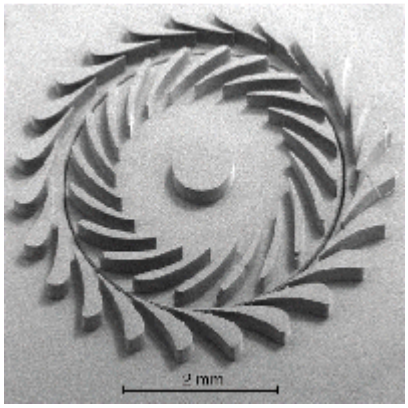

Figure 7. 4mm Diameter Micro-Scale Gas Turbine [9]

A new approach is required to develop individual power sources. Modern power devices operate in either the micro-scale range occupied by silicon MEMS or the macro-scale range occupied by traditional manufacturing techniques. Silicon MEMS are limited by fabrication technology in scaling power generation applications into larger devices with higher power output. Silicon is limited to the number of layers that can be used in fabrication. Ceramic tape technology and the development of Ceramic-MEMS (C-MEMS) offer an attractive alternative to both silicon MEMS and traditional fabrication technology. C-MEMS devices occupy the meso-scale device feature size in the millimeter range between the micro and macro size devices that is preferred for individual power generation while still taking advantage of processing techniques that allow for inexpensive batch fabrication.

C-MEMS devices provide a development platform that consists of internal, multi-layer channels and embedded metal materials in the same monolithic substrate. The

ceramic substrate is chemically and thermally resistant to harsh environments. Various metals can be embedded into the substrate to form chemical catalysts, electrical conductors, and thermal heat paths. Internal channels can be embedded inside the substrate to transport fluids through the device on many distinct layers. The capabilities of the C-MEMS materials platform allow the development of integrated systems that are the foundation of individual power generation devices. Low Temperature Co-Fired Ceramics (LTCC) is one ceramic material that is being used in this area of study. Researchers at Sandia National Laboratories have developed several devices that take advantage of this technology [10], which include 3D channels, inductors, and sensors.

Low Temperature Co-Fired Ceramics

Low Temperature Co-fired Ceramic (LTCC) materials are used in the electronics industry as a packaging material. Multi-layer LTCC has the capability of integrating circuitry into a hermetically sealed package: such as, resistive heaters, resistors, electrical connections, and inductors. LTCC is low cost and can be used for a broad range of applications. The advantages of LTCC for power generation were described by Plumlee [11].

The LTCC materials system used in this work was supplied by DuPont and is provided in the un-fired or “green state”. The LTCC substrate is composed of alumina, low temperature glass, and an organic binder according to DuPont [12]. While in this

state, the material can be machined, layered, and electrical circuitry incorporated. One advantage of LTCC is the capability for three dimensional structures. Vias, electrical connections between layers, can be used to connect circuits from one layer to the next. The use of vias protects circuitry on layers by hermetically sealing the layers. An Ion Mobility Spectrometer (IMS) prototype was developed by Plumlee et al. [13] with 66 ceramic layers. The IMS device uses multiple concentric rings to generate a constant electric field through a tube. Ions are presented into the electric field at one end and detected at the opposite end. The time required to traverse the length of the tube can be correlated to molecule size, and therefore chemical species can be determined. All of the rings have to be connected through the 66 layers using vias and each ring has an embedded resistor, which is used to create the electric field. This device is shown in Figure 8 and is one example of sensors being developed for use in the field and demonstrates the ability of LTCC to provide protection from harsh environments.

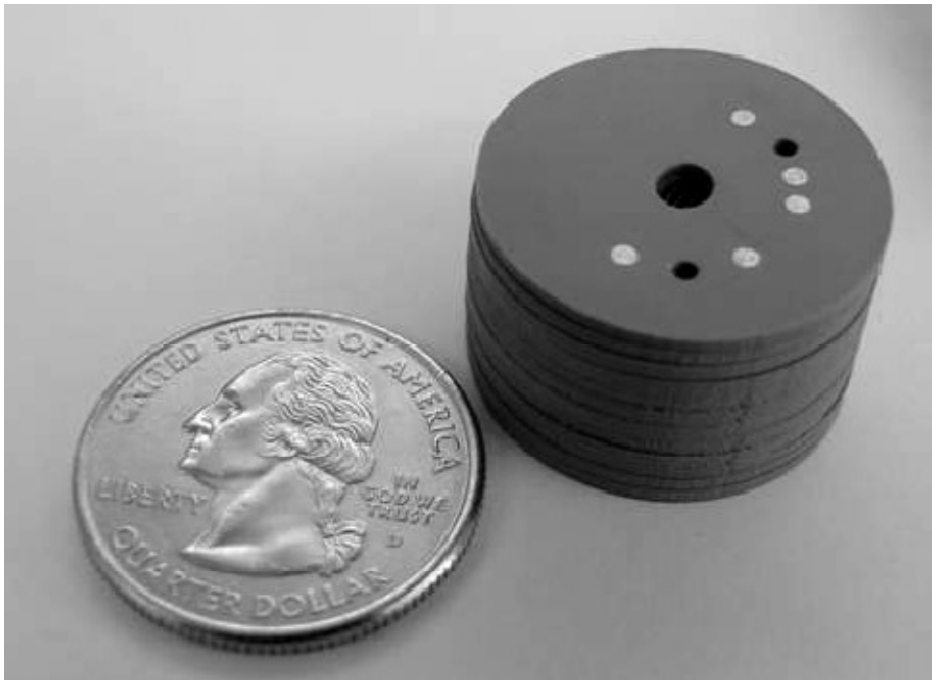

Figure 8. LTCC IMS with 66 Ceramic Layers [13]

The process for fabrication of a typical LTCC device is shown in Figure 9. The LTCC material supplied by DuPont is 0.254 mm thick sheets. A LASER milling machine is used to cut holes, vias, and cavities in the substrate. The LASER cut vias are filled with conductive paste using a stencil and knife blade. Conductive and resistor pastes are applied using a screen printer or direct writing system. Screen printers use a wire screen and squeegee to apply thick film paste in the pattern desired. The direct writing system dispenses paste onto the substrate in the pattern generated from a 3D model file. The ceramic layers are aligned and stacked together to be laminated in a vertical or isostatic press to 20.68 MPa. A uniaxial press laminates the LTCC from the

top and bottom in the vertical direction, whereas the isostatic press uses a water bath to press the part in all directions. Finally, the device is co-fired in a box furnace to 850°C, during this process the organic binder burns away and the glass sinters around the alumina participles forming the final device. This process is discussed in more depth during the fabrication section.

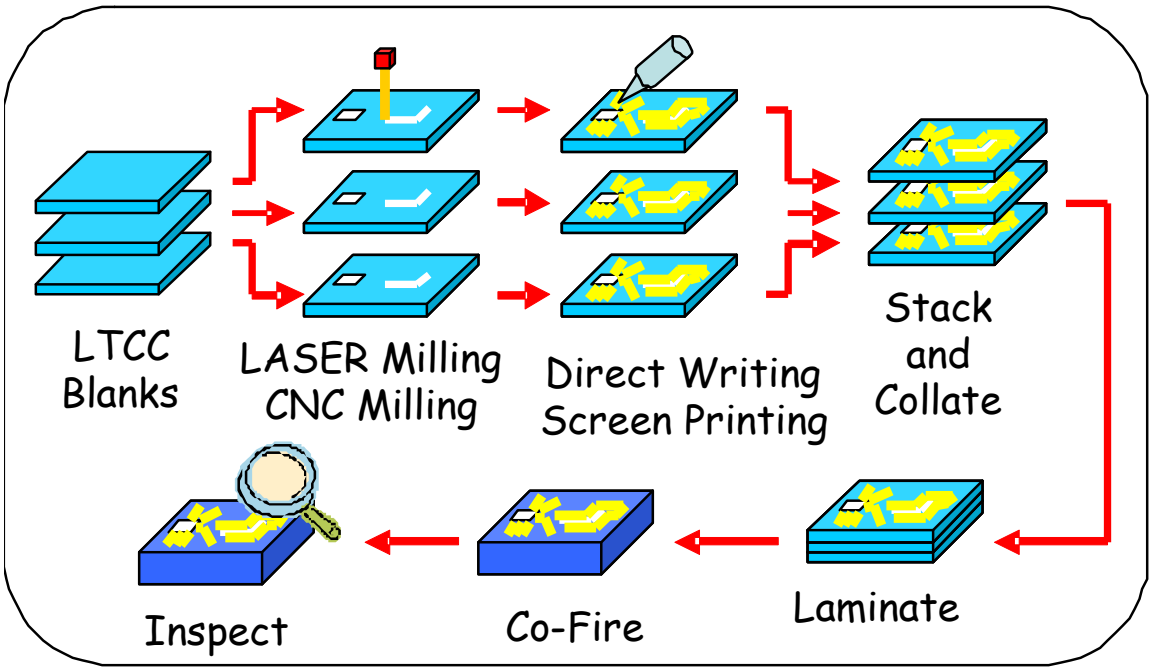

Figure 9. LTCC Process Flow [11]

Energy Scavenging Device (ESD)

An energy scavenging device (ESD) extracts energy from ambient movement in the environment. Specific applications of this type of device range from the piezoelectric

shoe demonstrated by Shenck and Paradiso [7] to the gear and pinion backpack described by Rome et al. [14]. The energy generation used in the Rome backpack shown in Figure 10 is an example of a traditional solution to energy scavenging. The Rome backpack suspends the pack load on a set of springs. The load is allowed to oscillate on rods and bushings while the wearer is walking. The energy in the oscillations is extracted using a rack and pinion gear system attached to a rotary generator similar to a car alternator. As the pack moves up and down, the toothed rack spins the pinion on the generator clockwise and then counterclockwise. The generator output power is then rectified to produce a smooth DC output voltage that is used to charge a set of onboard batteries. This design is an example of an adaptation of current technology for a remote power source. The rotary generator is commonly used in turbines and alternators where the driving power source is rotational motion in the form of a turning shaft.

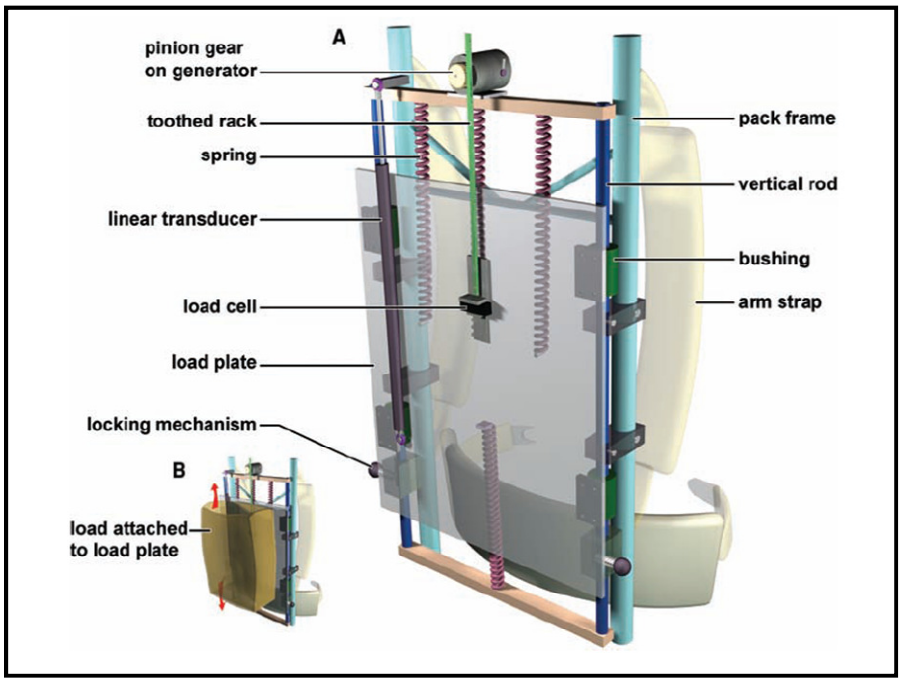

Figure 10. Rack and Pinion Generator on a Backpack [14]

Using a traditional rotary generator to extract energy from the linear movement of a backpack is inefficient and complicated. The multiple moving parts associated with a rack/pinion/generator system substantially decrease the reliability of the device. The exposure of the moving generator parts to the sand, ice, and rain found in harsh environments accelerates corrosion, along with frictional wear. Any misalignments in the system due to damage could render the generator system ineffective. The numerous parts required for implementation substantially increase the overall system weight. Also, the added inertia of the rack/pinion/rotary generator system limits the ability to extract usable power from the pack oscillations. Combining these technological challenges limits the functionality of the Rome backpack in a real world environment.

Attempting to convert the oscillations from the backpack into power through a rotary generator system is inefficient and ignores the link between the linear direction of the oscillation and linear power generation. An alternative design can be found in large scale power generation systems designed to extract energy from ocean waves as described in Figure 11. These energy scavengers convert the linear motion of a floating buoy rising and falling into a linear generator tethered to the ocean floor.

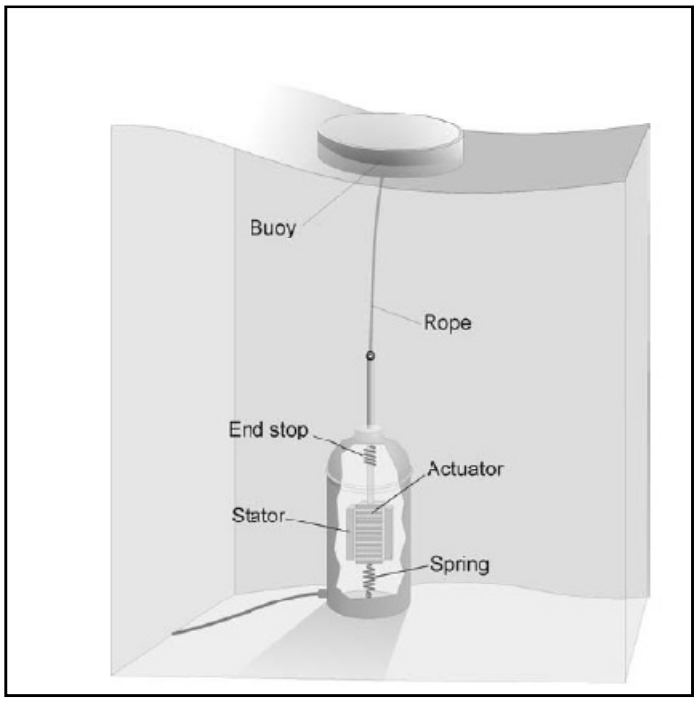

Figure 11. Linear Generator Developed for Wave Energy Extraction [15]

This group of energy scavenger devices relies on the movement of a linear magnetic armature inside a linear coil to produce power by electromagnetic induction. The number and size of the magnets and axial coils in the device determines the magnetic

reacting force and thus the generated power. A 100kW device was recently proposed by Ivanova et al. [16]. Danielsson et al. and Baker et al. have published several papers on the design and selection of various types of linear generator concepts [17], [18]. Mueller and Baker have presented a performance model for the large wave motion devices [19]. Wang et al has developed a similar model for a meso-scale tubular linear generator using this same methodology [20]. This miniature device shown in Figure 12 produces an output power of 15 mW with a magnet radius of 2.4 mm.

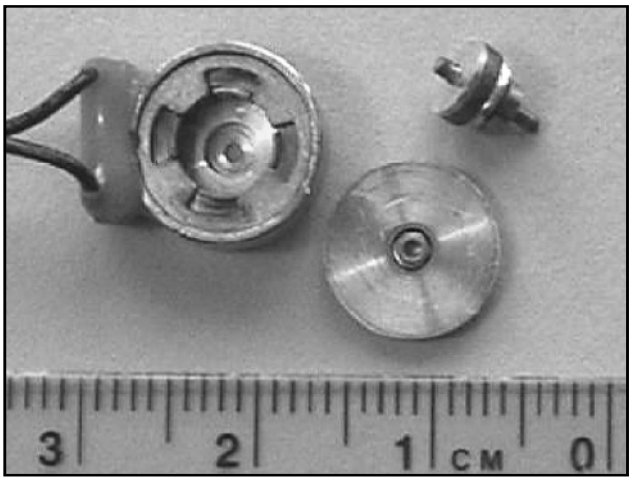

Figure 12. Single Pole Prototype Linear Generator [20]

Electromagnetic Generator Integrated into a Backpack

According to Saunders, et al. [21], walking motion can be simplified to the movement of an inverted pendulum. As the person steps down, the body pushes up off the floor and jumps over the foot. The center of mass displaces a vertical distance of 4-7

cm [22], shown in Figure 13. The frequency a normal person walks at is 2 Hz, which was determined by Rome et al. [14]. Also, the backpack has a load between 20 kg and 38 kg, which was determined by the standard weight of a backpack also found by Rome et al. [14].

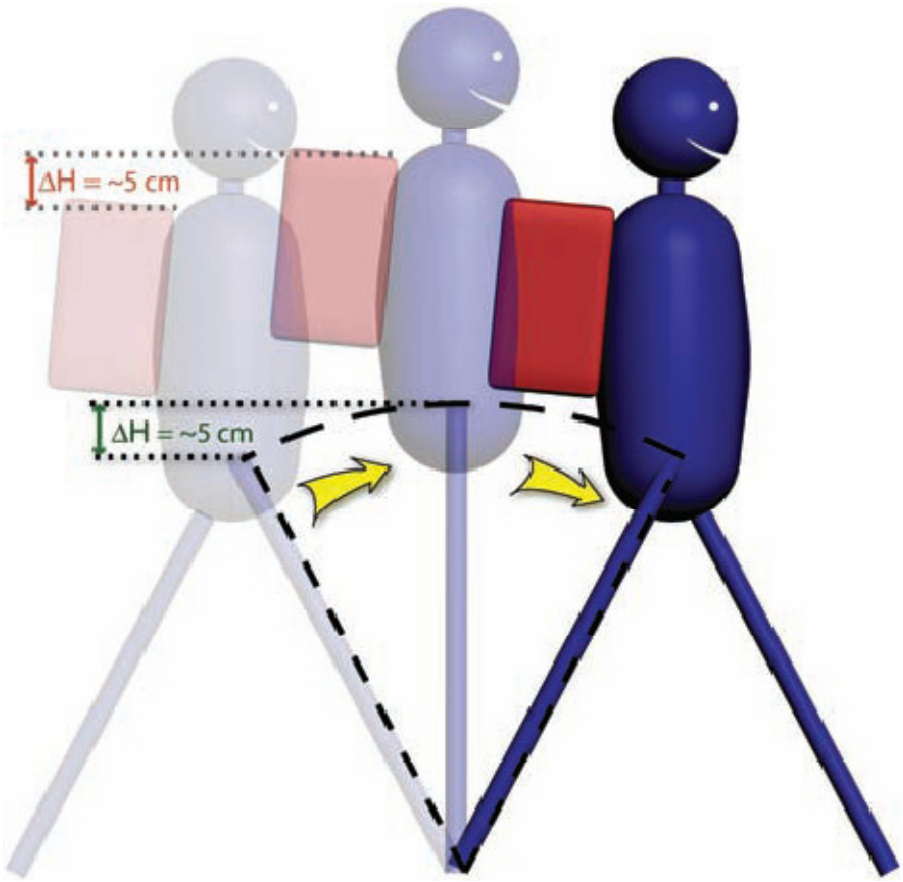

Figure 13. Walking Motion Modeled as an Inverted Pendulum [14]

Two miniature tubular linear electrical generator devices similar to those proposed by Mueller and Baker [19] will be integrated into the sliding pack saddle. The saddle and pack will be suspended on springs and slide on a tubular frame attached to a harness system, not shown in Figure 14. The only contact with the frame occurs through slide bushings (4). The linear scavengers (2) are mounted as shown in Figure 14. The magnetic armature is fixed in the tubular frame and the coils are positioned in the pack saddle. No physical contact occurs between the armature and the coils. The relative movement between the armature and the coils generates a magnetic reacting force that induces a voltage in the device. This alternating output is then rectified and stored internally in a battery. The backpack design and testing of the generator are not in the scope of this thesis and will be studied in future work.

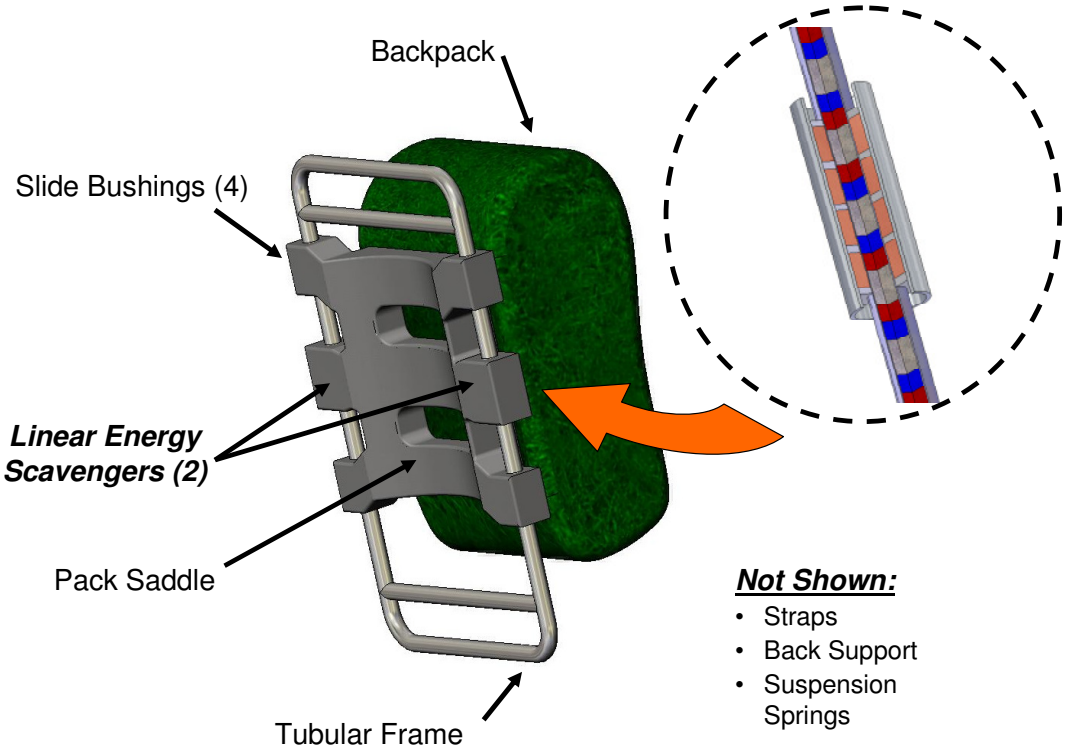

Figure 14. Backpack with Integrated Miniature Linear Electric Generators

The linear electric generator concept is shown in more detail in Figure 15. The armature is composed of a series of rare earth (Neodymium) magnets positioned axially. The magnets are shown in the figure as blue and red blocks. The red end is schematically the north magnetic pole and the blue is the south magnetic pole. The magnets are positioned with two north poles facing each other and are separated by a ferroelectric iron spacer. The south poles are also facing each other separated by an iron spacer. The coils are positioned cylindrically around the armature with a small air gap separating the inner

coil from the protective sheath. The coils are fabricated using ceramic tape technology to produce a high density coil that is resistant to harsh environments.

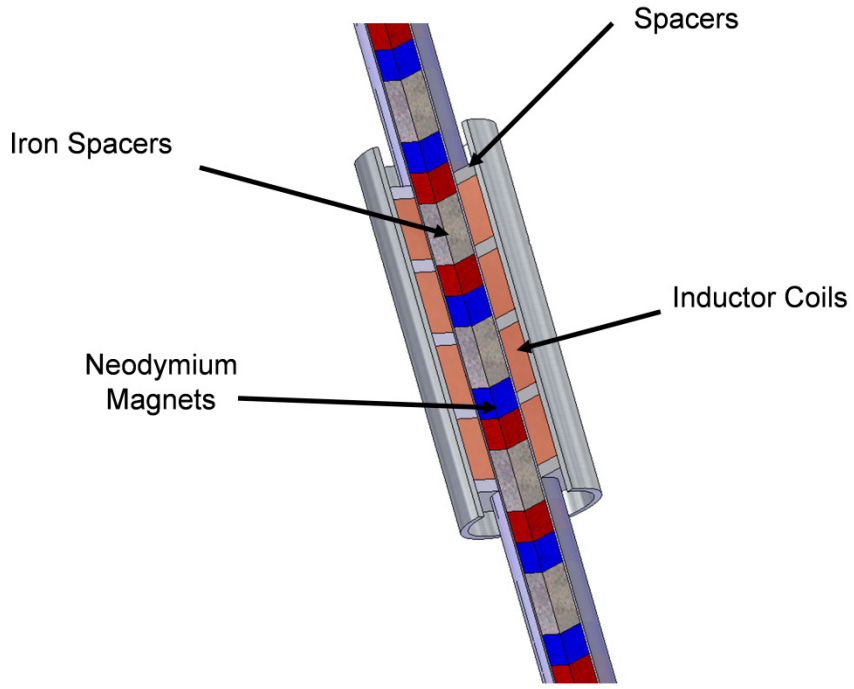

Figure 15. Linear Electric Generator Concept

The predicted magnetic flux circuit and device cross-section are shown in Figure 16. As described by Mueller and Baker [19], the opposing magnets generate a magnetic flux pattern that propagates radially through each coil. As the magnetic armature moves through the coils, the flux direction alternates rapidly, thus generating an output power. This system should be designed to be effective at various speeds and oscillation amplitudes, particularly in the range of motion similar to human walking.

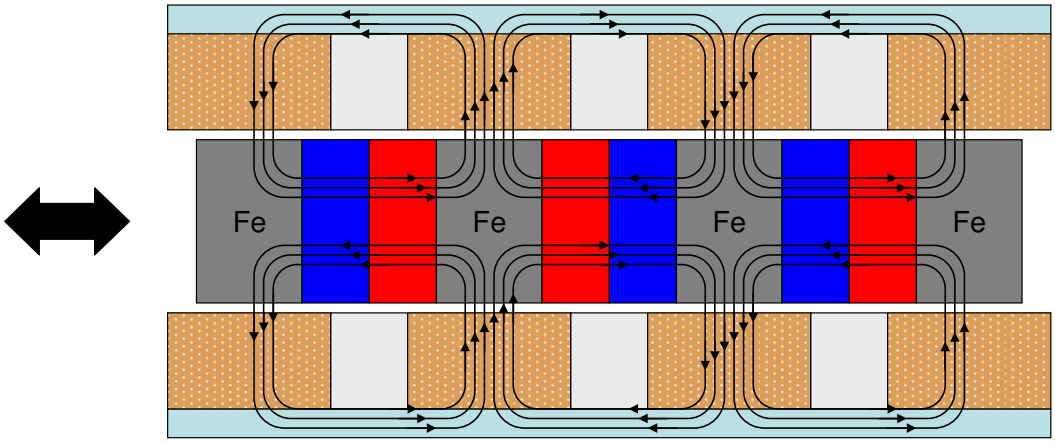

Figure 16. Linear Electric Generator Cross Section with Flux Lines

Thesis Description

For this project, a linear electromagnetic generator was modeled and designed for use in a backpack configuration to charge small portable devices, reducing the need for batteries. Compared to the Rome et al. [14] backpack, the device is a direct conversion of a linear oscillation into a usable power output. If the losses are less when using a direct conversion of linear oscillation, then the device will produce a higher peak power output than the rack and pinion.

The electromagnetic generator design has several advantages over the rotary generator concept being developed by Rome et al. [14]. The lack of a rack and pinion gearing apparatus significantly reduces the frictional losses in the system. There is no

rotational inertia to overcome in the linear system as compared to the rotary generator and gearing approach. The non-contact linear magnetic induction allows the coil and magnetic armature to be protected from sources of corrosion such as dirt, water and ice. The linear inductive sliding mechanism can tolerate more misalignment if the tubular frame is bent. Fewer moving parts reduce the overall complexity and weight of the application. The advantages of the linear inductive system demonstrate the potential of this application as compared to the rotary generator system.

The development of the generator starts with an analytical model that describes the mechanical and magnetic systems. The mechanical system is a model of the vibration of the physical system, which is used to predict the amount of available power that can be generated by walking with a backpack. Because of the complexity of the magnetic system, a model developed by Baker [23] was chosen to determine the power being produced by the electromagnetic generator. A Simulink model completes the analytic model to determine the design requirements of the generator. The design of the generator is discussed in the following section, including a detailed design.

ANALYTIC MODEL

An analytical model of the backpack's motion and the generator is vital to the project. The model predicts the available power generated from the walking motion and the amount of power the electromagnetic generator can produce. Some constraints on the system are the size and weight of the generator. The purpose of the generator is to reduce the need for batteries, which can be heavy and expensive. The model is optimized for a 2 Hz walking speed, which is the speed of a brisk walk. The weight of the backpack was set to 28 kg, standard weight of a military backpack [14]. The backpack should also not prevent the wearer from using a normal walking motion.

The backpack suspends the pack load on a set of springs. The load is allowed to oscillate on rails and linear bearings while the wearer is walking. The magnets and spacers are attached to the person, and are moving with the base of the mechanical model. This means that the coils are attached to the backpack and are moving with the same frequency as the backpack. As the coils move past the magnetic armature, the flux direction alternates rapidly, thus inducing a current.

The physical system is modeled in two parts. First the mechanical model is presented. The results of the mechanical model are used in the development of the electromagnetic model. As the coil generates power, it is extracting energy, which can be

modeled as a damping force. Another type of force that acts like this is a viscous damper; it converts the energy into heat instead of voltage. The generator damping ratio of the system is the link between the Mechanical Model and the Magnetic Model. The relative velocity, difference between the velocity of backpack and the person, is calculated using the mechanical model and then used in the magnetic model to calculate the magnetic force. As the generator removes energy from the system, it changes the relative velocity. An iterative process was needed to calculate the peak magnetic force accurately by starting with a damping ratio and calculating the relative velocity. The relative velocity was then used in the magnetic model to calculate the peak force from the coils. From the peak force, a damping ratio was calculated and if the ratio matched the original damping ratio, then iteration was complete; and if the damping ratios were not equal, the iteration process was repeated using the new calculated damping ratio until the ratios were the same. A schematic of the process is shown in Figure 17.

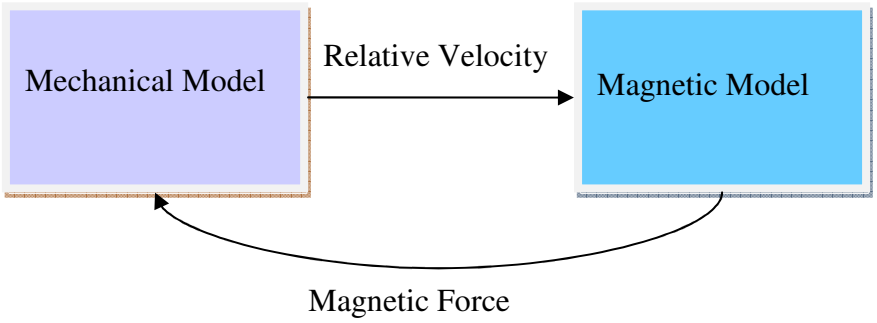

Figure 17. Schematic of Analytic Model

Mechanical Model

A mechanical model was used to determine the vibration and movement of the backpack in order to predict the voltage and maximum power available from the system. The backpack is modeled as a base excitation vibration model, shown in Figure 18. Base excitation was chosen because the backpack is being excited by the harmonic displacement of the person's walking movement. Base excitation is the model of force acting through a spring and damper on a mass, displayed in Figure 18. The shocks of an automobile are one example of a base excitation system. The generator will take advantage of the base excitation functionality of producing larger oscillation amplitudes of the mass with smaller input amplitudes from the base. The backpack has greater amplitude than the amplitude of the person's center of mass. This modeling approach for the backpack system was also used by Xu et al. [24].

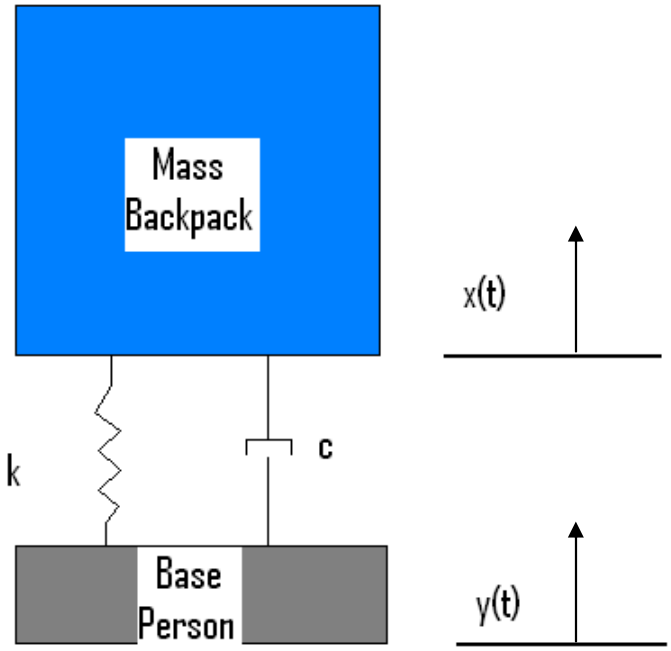

Figure 18. Base Excitation Model

The equations used in the model are from Inman [25]. Some general equations needed in analysis are natural frequency and damping ratio. Natural frequency, ω_n, is the frequency the backpack system will oscillate when set into motion without any interference from external forces; see Equation (1), with k defined as the stiffness of the spring and m defined as the mass of the system. The damping ratio, ξ, characterizes how the oscillation amplitude of the backpack system will decay due to conservative forces. Equation (2) shows the relationship between the damping ratio, ξ, and damping coefficient, c, mass, m, and natural frequency, ω_n.

$$\omega_n = \sqrt{\frac{k}{m}} \tag{1}$$

$$\xi = \frac{c}{2m\omega_n} \tag{2}$$

Summing the forces on the mass yields Equation (3), with $\ddot{x}$ and $\dot{x}$ being the acceleration and velocity, respectively, of the mass of the backpack.

$$m\ddot{x} + c(\dot{x} - \dot{y}) + k(x - y) = 0 \tag{3}$$

Assuming the person walks with a harmonic output, the displacement of the base, ***y(t)***, as a function of time, ***t***, is shown in Equation (4). ***Y*** is the amplitude of the base and ω_b is the frequency of the person walking. The frequency ratio, ***r***, Equation (5), is the ratio of frequency of the base, ω_b, and the natural frequency, ω_n.

$$y(t) = Ysin(\omega_b t) \tag{4}$$

$$r = \frac{\omega_b}{\omega_n} \tag{5}$$

Inserting Equation (4) into Equation (3), taking the derivative of Equation (4) and using the definition of natural frequency ω_n and damping ratio ξ, the equation of motion becomes Equation (6).

$$\ddot{x} + 2\xi\omega_n\dot{x} + \omega_n^2 x = 2\xi\omega_n\omega_b Ycos(\omega_b t) + \omega_n^2 Ysin(\omega_b t) \tag{6}$$

Equation (6) is analogous to a basic spring-mass-damper system with two external forces on the system. The solution to Equation (6) is the sum of the particular solution for each harmonic sine and cosine excitation. From the principle of linear superposition, the particular solution, $\boldsymbol{x_p(t)}$, of Equation (6) is Equation (7). To find the particular solution, $\boldsymbol{x_p(t)}$, the method of undetermined coefficients is used. The method of undetermined coefficients is the process of finding the solution of an inhomogeneous ordinary differential equation by separating it into two homogeneous ordinary differential equations and finding the solution to the homogenous equations. Each solution is shown in Equation (8) and Equation (9), with $\boldsymbol{\vartheta_1}$ defined as the phase shift, shown in Equation (10).

$$x_p(t) = x_p^1 + x_p^2 \tag{7}$$

$$x_p^1 = \frac{2\xi\omega_n\omega_b Y}{\sqrt{\left(\omega_n^2-\omega_b^2\right)^2+(2\xi\omega_n\omega_b)^2}} cos(\omega_b t - \theta_1) \tag{8}$$

$$x_p^2 = \frac{\omega_n^2 Y}{\sqrt{\left(\omega_n^2-\omega_b^2\right)^2+(2\xi\omega_n\omega_b)^2}} sin(\omega_b t - \theta_1) \tag{9}$$

$$\theta_1 = tan^{-1}\left(\frac{2\xi\omega_n\omega_b}{\omega_n^2-\omega_b^2}\right) \tag{10}$$

Summing Equation (8) and Equation (9) and using the properties of linear combination of sine and cosine with the same frequency, Equation (7) becomes Equation

(11), with $\boldsymbol{\vartheta_2}$ defined as the phase shift from combining sine and cosine, shown in Equation (12).

$$x_p(t) = \omega_f Y \sqrt{\frac{\omega_n^2+(2\xi\omega_b)^2}{\left(\omega_n^2-\omega_b^2\right)^2+(2\xi\omega_n\omega_b)^2}} cos(\omega_b t - \theta_1 - \theta_2) \tag{11}$$

$$\theta_2 = tan^{-1}\left(\frac{\omega_n}{2\xi\omega_b}\right) \tag{12}$$

Substitute $\boldsymbol{\omega_f}$ and $\boldsymbol{\omega_b}$ from Equation (11) with the frequency ratio, $\boldsymbol{r}$, seen in Equation (5). The simplified particular solution becomes Equation (13), with the magnitude, $\boldsymbol{X}$, of the particular solution shown in Equation (14).

$$x_p(t) = Xcos(\omega_b t - \theta_1 - \theta_2) \tag{13}$$

$$X = Y\sqrt{\frac{1+(2\xi r)^2}{(1-r^2)^2+(2\xi r)^2}} \tag{14}$$

Using these equations, it was found that oscillation at high frequencies (r>1) with a large mass would be highly detrimental to the person walking because of the high forces transmitted to the person as shown in Figure 19. The transmitted force is calculated using Equation (15), which is the reaction force of the force acting through the spring and damper on the mass. A value of 100 N was selected as the maximum transmitted force to the person to limit how the backpack will affect the person's walking motion. Thus, a value less than 1 was chosen for the frequency ratio ($\boldsymbol{r}$<1).

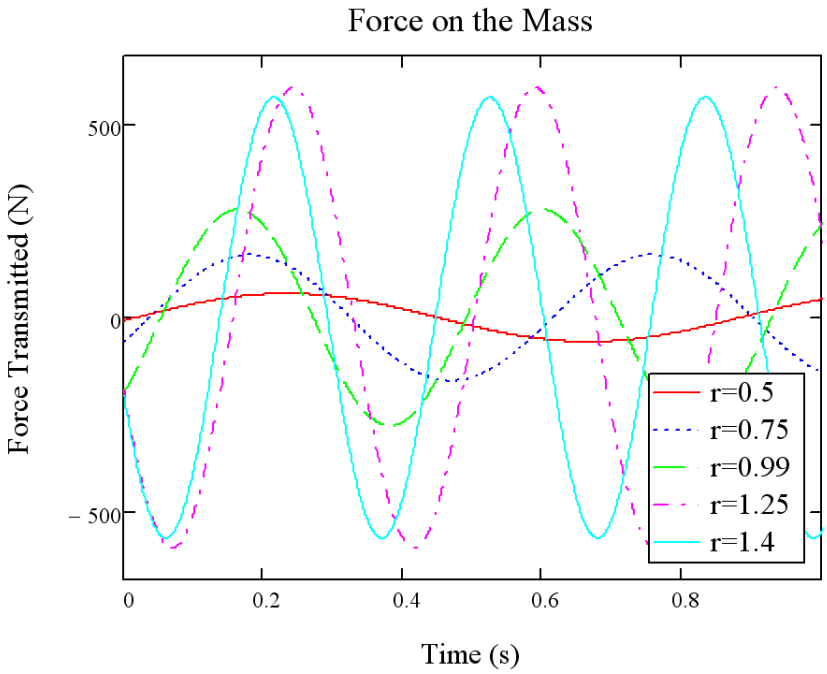

Figure 19. Force Transmitted to the Person

$$F_T(t) = k\big(x_p(t) - y(t)\big) + c\big(\dot{x}_p(t) - \dot{y}(t)\big) \tag{15}$$

The relative backpack velocity, backpack velocity minus the person (base) velocity in the vertical direction, Equation (16), is shown in Figure 20 in time. Figure 20 indicates that the relative velocity is larger for larger frequency ratios. If the backpack and person had the same velocity, Δv=0, the magnets and coils would be moving together and not producing any power. With larger relative velocity, the energy that will be available to extract from the system increases.

$$\Delta v(t) = \dot{x_p}(t) - \dot{y}(t) \tag{16}$$

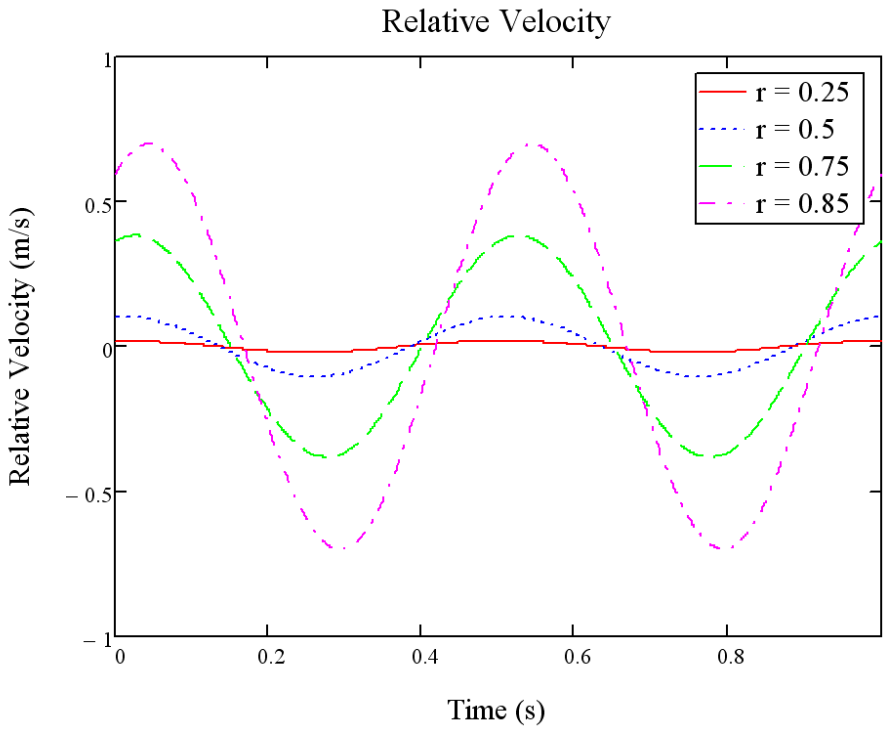

Figure 20. Relative Velocity of Person and Backpack

In order to observe the effect of the frequency ratio on the power output, the Root Mean Square (RMS) Power was calculated from relative velocity as shown in Equation (17). Power is work divided by time and the work being done is through energy extraction by the electromagnetic generator. The work is force times distance and the force is the damping coefficient times the RMS velocity. Useful work is generated from the conservative force of the electromagnetic generator. The damping coefficient couples to the magnetic model because it is the magnetic force. So the available RMS power is shown in Equation (18). The frequency ratio is determined using the plot of the RMS

power vs. the damping ratio. Also, this plot shown in Figure 21 shows a peak RMS power for each particular damping ratio. For a frequency ratio of 0.8, there is a peak RMS power of 16 watts corresponding to a damping ratio of 0.25. The peak is found for relatively small damping ratios.

$$\Delta v_{rms} = \sqrt{\frac{1}{T_2 - T_1}\int_{T_1}^{T_2} \Delta v^2 dt} \tag{17}$$

$$P_{rms} = c\Delta v_{rms}^2 \tag{18}$$

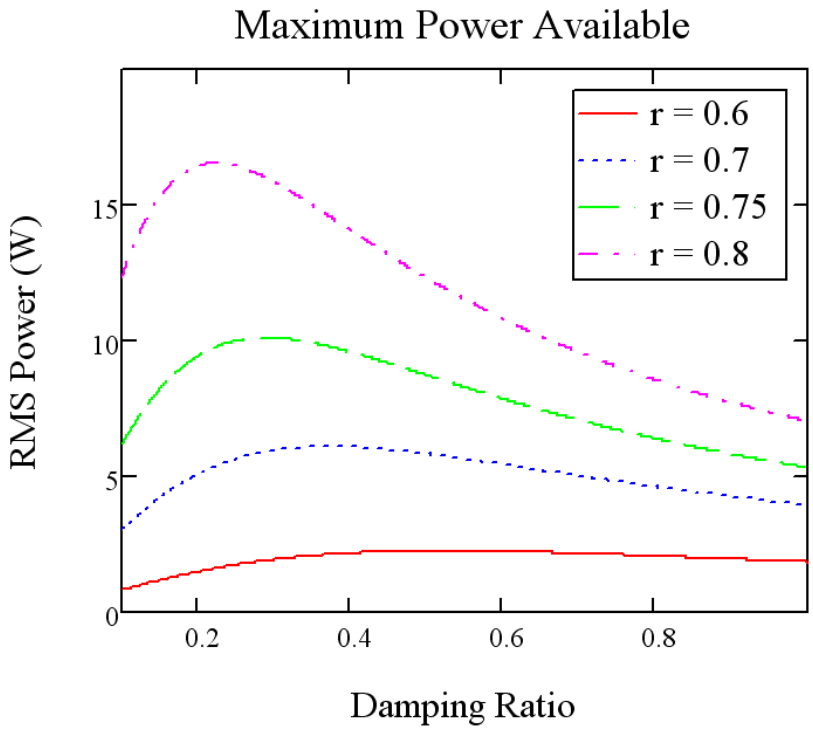

Figure 21. Maximum RMS Power Available

From the relative velocity, Equation (16), and maximum RMS power, Figure 21, a value of r=0.743 was chosen to maximize the relative velocity without reaching resonant frequency (r=1) to reduce the force transmitted to the person wearing the backpack. A spring constant of 8kN/m was calculated to achieve this frequency ratio. The damping ratio includes the magnetic force generated from the induced current. The magnetic force acts like a damper by taking energy out of the system; it opposes the base force by the person.

Magnetic Model

The power generation produced by Mueller and Baker [19] from wave motion is used as the model for the magnetic system, specifically the ironless tubular generator proposed in Baker's doctorial dissertation [23]. From Knight [26], Faraday's Law states that current is induced in a coil when it is passed through a changing magnetic field. The opposing magnets generate a magnetic flux pattern that propagates radially through each coil, shown in Figure 22. The axial force, force in the $\boldsymbol{y}$ direction, is maximized at the steel spacers and the radial force, force in the $\boldsymbol{z}$ direction, is maximized at the center of the magnets. The coil configuration is shown in Figure 23. Force is developed as a result of current flowing through the coils, which are situated in the magnetic field of the stator. The direction of this force is mutually orthogonal to the current and field strength and has a magnitude of their product multiplied by the length of conductor in the field, from Baker [23], shown in Equation (19).

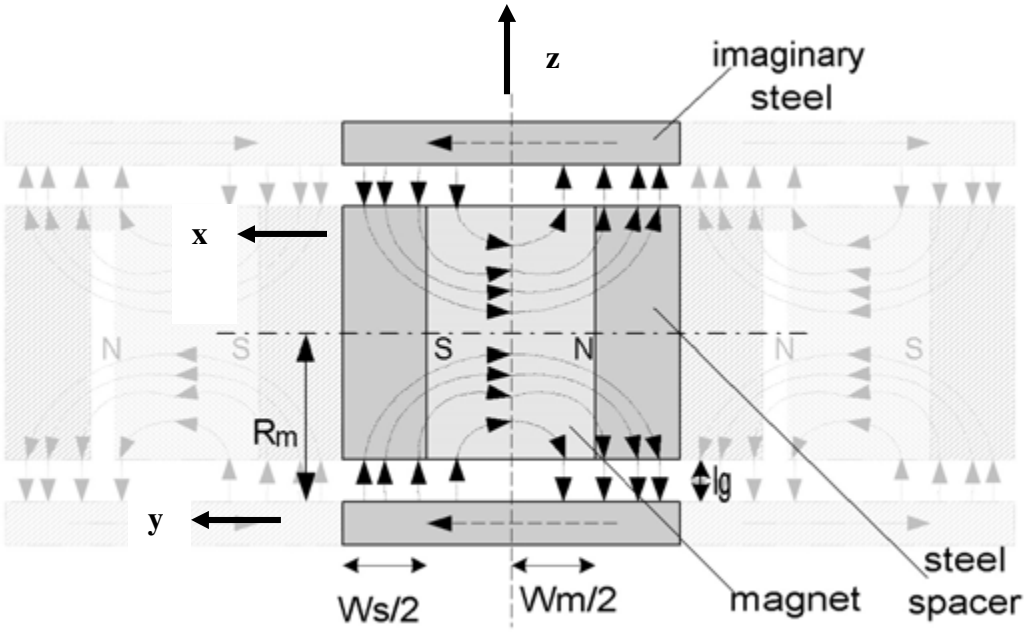

Figure 22. Baker [23] Simplified Magnetic Flux Lines

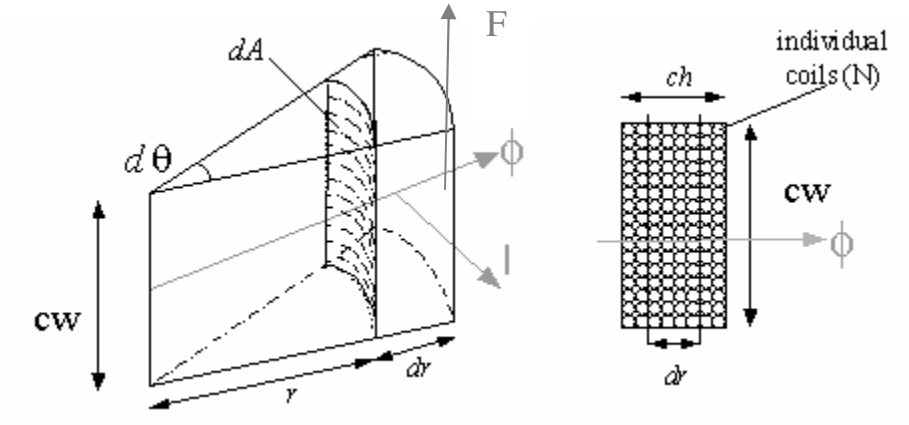

Figure 23. Baker [23] Coil Configuration

$$F = I \times \varphi \tag{19}$$

For this model, several constants are introduced to characterize the coil geometry. The outer radius of the coil is a function of the magnet radius, air gap, and coil thickness, shown in Equation (20). The Inner radius of the coil is shown in Equation (21), where $\boldsymbol{R_m}$ is the magnet radius and ***gap*** is the air gap between the magnets and coil. The last constant is the volume of the coil shown in Equation (22).

$$R_o = R_m + gap + ch \tag{20}$$

$$R_i = R_m + gap \tag{21}$$

$$volume = \pi cw(R_o^2 - R_i^2) \tag{22}$$

The proposed system does not use steel on the outside of the device, but in order to calculate the flux, an effective air gap needs to be calculated that will give the same reluctance as if the steel were present as shown by Baker [23]. From Equation (23), the effective air gap is calculated using the magnet and steel spacer widths. The flux is calculated in Equation (24) using the remnant flux density, $\boldsymbol{B_r}$, geometric constants, and the relative permeability. The flux density at the surface of the rotor is calculated using Equation (25). Equation (26) comes from the model developed by Baker [23], which assumes the flux density has an exponential decay with radius across the coil area. The flux density is a function of the flux density at the surface of the magnets, Equation (25), the coil and magnet radius, and the effective air gap, Equation (23).

$$l_g = \frac{w_m + w_s}{\pi} \tag{23}$$

$$\varphi_p = \frac{\pi^2 B_r w_m w_s R_m^2}{2\mu_r R_m(w_m+w_s)+\pi w_m w_s} \tag{24}$$

$$B_g = \frac{\pi B_r R_m w_m}{2\mu_r R_m(w_m+w_s)+\pi w_m w_s} \tag{25}$$

$$B(R) = B_g exp\left(\frac{-R+R_m}{l_g}\right) \tag{26}$$

From the effective air gap and the flux density, the value of the coil radius can be calculated by setting the flux density at the outer surface of the coil to be 25% of the flux density at the surface of the rotor and solving for the radius. The induced current is calculated from Ohm's law [26] as seen in Equation (27) and Equation (28).

$$I_c = \frac{\Delta v L_p B(R)}{Resistance} \tag{27}$$

$$J_c = \frac{I_c L_p}{volume} \tag{28}$$

Peak force on the coils from the magnetic field can be calculated using the model developed by Baker [23] by taking the integral over the volume of the coil, Equation (29). This is a peak force and does not take into account the changing magnetic field as the coil moves through the magnetic field, but the peak force does include the number of coils to calculate the path length $\boldsymbol{l_g}$. Equation (30) is the integration of the peak coil force of Equation (29).

$$F_c = \int_0^{2\pi} \int_{R_i}^{R_o} \int_0^{cw} J_c B(R) R dz dR d\theta \tag{29}$$

$$F_c = \frac{\pi c w \Delta v L_p^2 B_g^2 l_g \left[2R_i + l_g - (2R_o + l_g) e^{\frac{-2ch}{l_g}}\right] e^{\frac{-2gap}{l_g}}}{2Resistance * Volume} \quad (30)$$

Figure 24 shows the peak force as a function of time and the damping ratio ($\boldsymbol{\xi}$). The response is oscillatory with decreasing amplitude with increasing damping ratio; with a small damping ratio, the relative velocity is larger. The peak force has a tradeoff between extracting the most amount of energy from the system and extracting too much energy, which slows down the system. If the system's relative velocity is low, the peak force will decrease. Each response has a different frequency due to the phase shift described in Equation (10), which is a function of the damping ratio. For the calculations of force and power, the number of coils is set to 480.

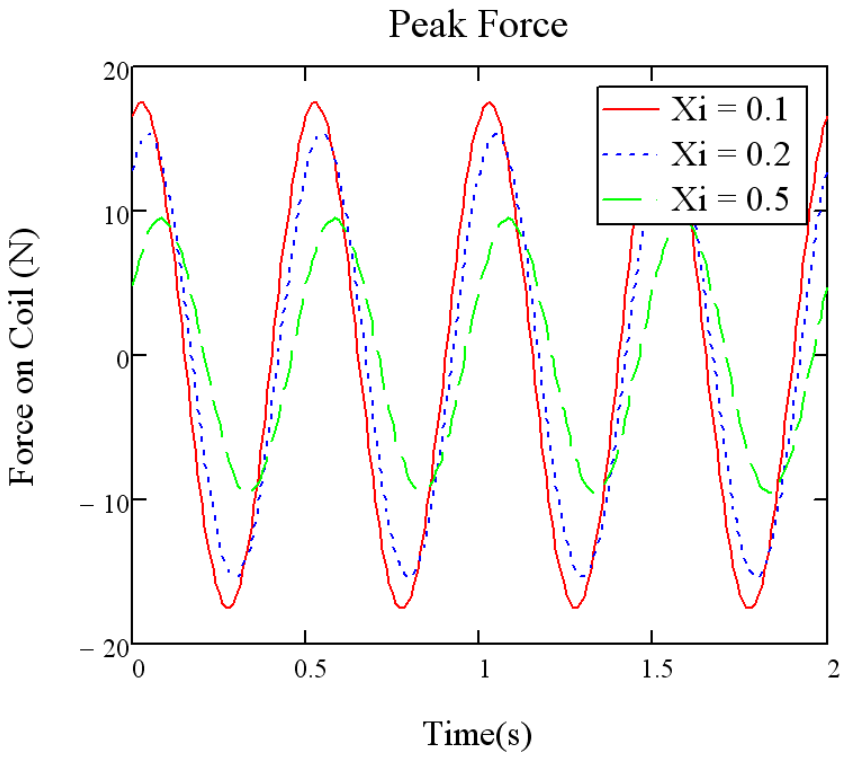

Figure 24. Peak Force from Coil

The power generated by the magnetic force is shown in Figure 25. Power generated is the magnetic force in the coil times the relative velocity. Figure 25 also shows that a smaller damping ratio gives a larger power output, with a peak around 4 watts. The response is oscillating power and has different frequencies for each damping ratio.

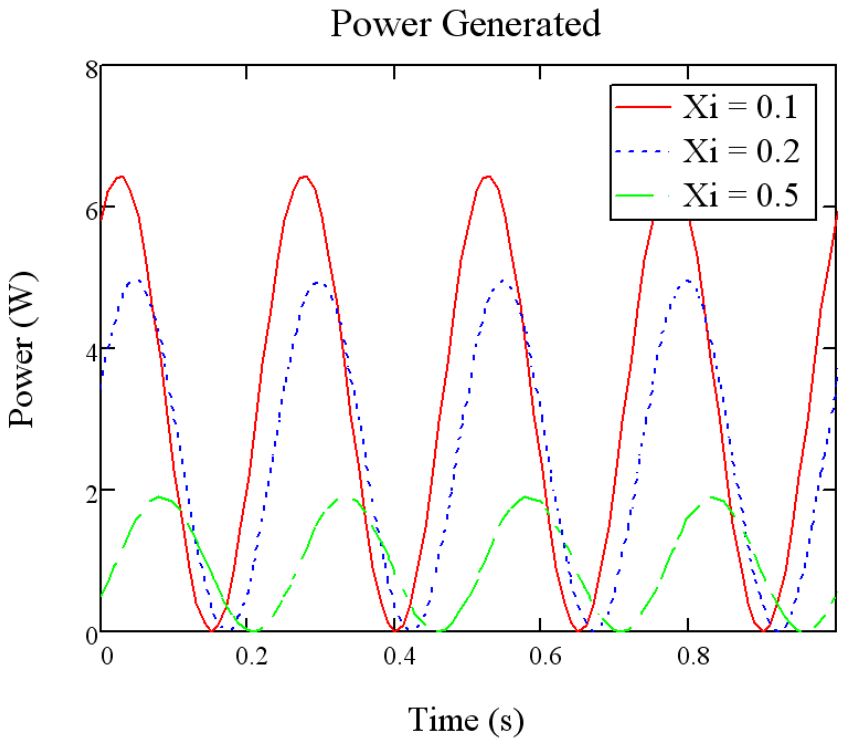

Figure 25. Rectified Power Generated in Coil from Inductance

The force and power calculations are peak values when the coil is positioned at the steel spacer and do not change with position. The flux density is changing with position, shown in Figure 26. The valley is when the coil is positioned at the center of the magnet and the peak is at the center of the steel spacer. The instantaneous magnetic force and power are shown in Figure 27 and Figure 28, respectively. As the coil passes the magnet, the force and power drop to zero and the peak value is the same as the values shown in Figure 24 and Figure 25. When the coil is experiencing the maximum velocity,

it is at the center of the rotor and has the highest peak value. Each drop to zero represents the coil passing a magnet. In one cycle, the coil passes five magnets.

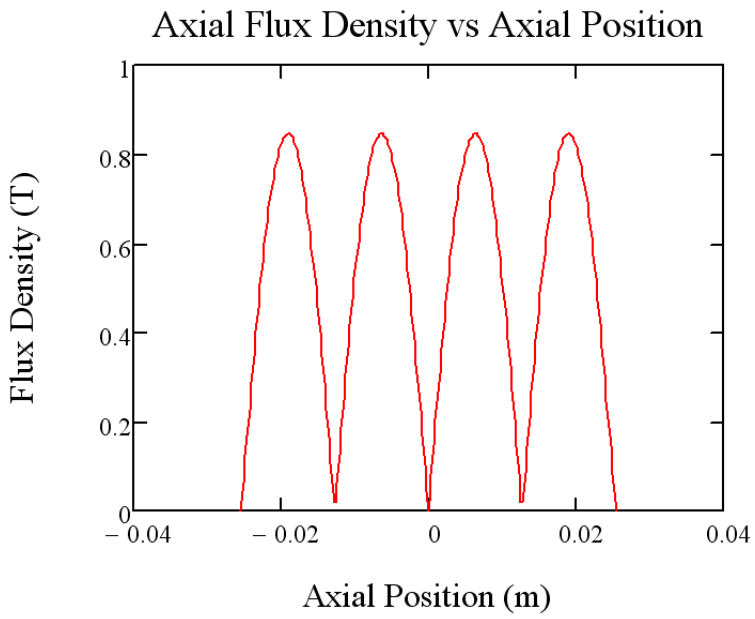

Figure 26. Axial Flux Density as a Function of Axial Position

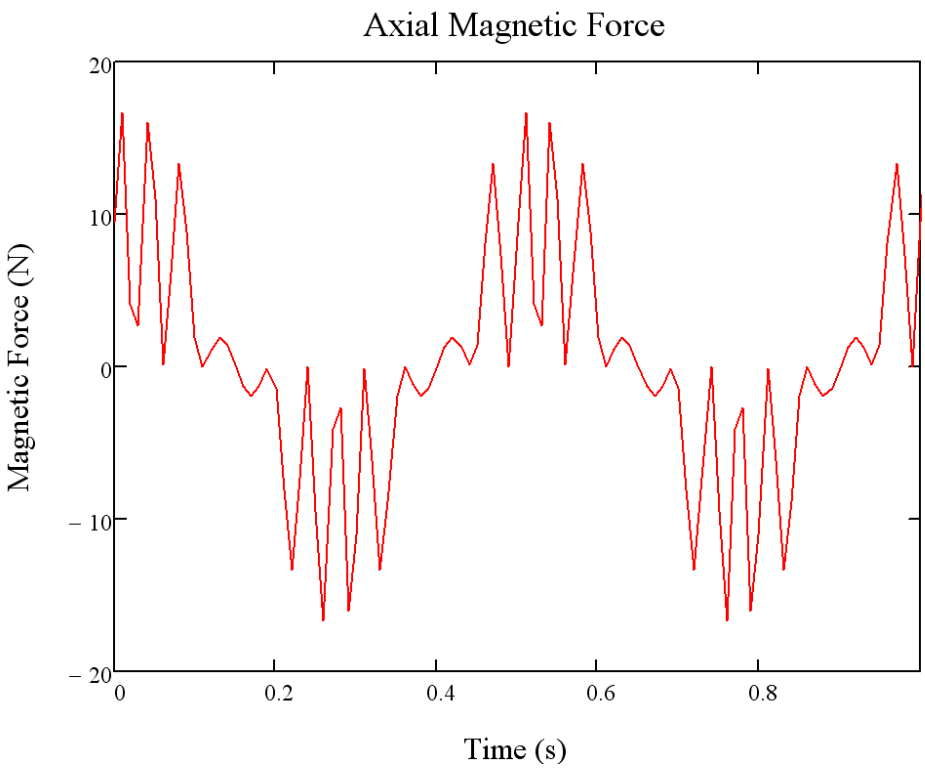

Figure 27. Axial Magnetic Force

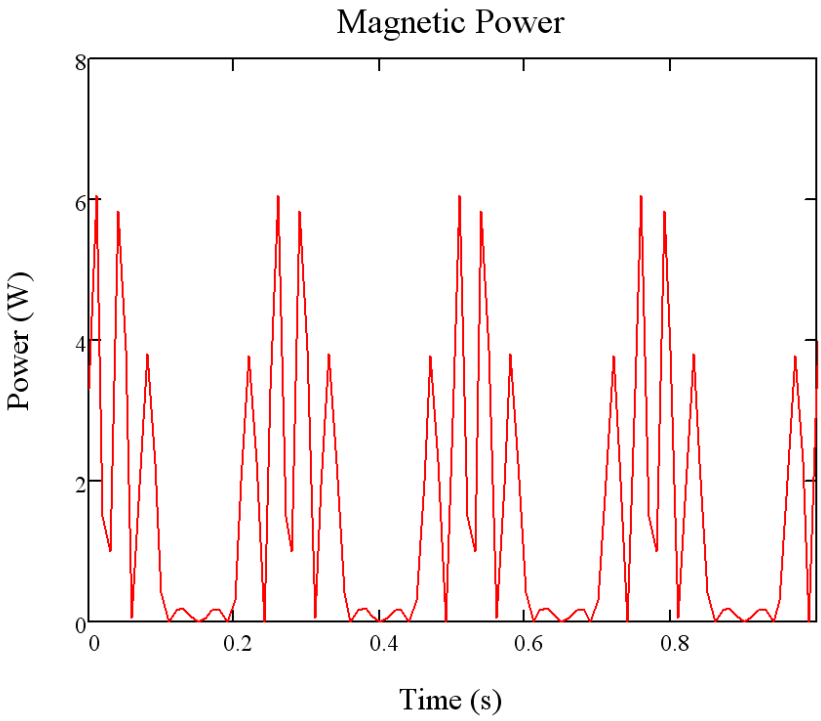

Figure 28. Instantaneous Generated Magnetic Power

The magnetic model gives a reasonable estimate for the power that the generator can produce based on the available power calculated in the mechanical model. It also provided guidance in determining the number of inductor coils and the overall dimensions of the device discussed in the design section. A more complex model of the analytical solution was created from this geometry by Wang et al. [27].

SIMULINK MODEL

The Simulink model was used to verify the equations of motion used in both the mechanical and magnetic models. Also, Simulink shows the transient response of the system and that it dies out quickly. The difference in the Simulink model is in the de-coupling of the magnetic force, which is separated from the damping coefficient for simplification in the analytical model. The damping force in the Simulink model is the friction generated by the movement of the backpack. The damping coefficient is set to ξ=0.1 and would need to be found experimentally in the actual apparatus. Also, the Simulink model replaces the relative position and velocity with z, shown in Equation (31). The equation of motion is shown in Equation (32).

$$z = x - y \tag{31}$$

$$m\frac{d^2z}{dt^2} + c\frac{dz}{dt} + kz = -mY\omega_b^2 sin(\omega_b t) - F_{mag} \tag{32}$$

The Simulink model is shown in Figure 29. The input force is the force from the person (base) walking, which is being transmitted through the spring and damper. The damping ratio from friction was set to ξ=0.1. The relative velocity of the base and backpack is used to determine the magnetic force. The script file for the MATLAB Function of magnetic force is in Appendix B. The magnetic force is summed with the input force, damping force, and spring force. The summation is then integrated twice to

solve for the relative position of the backpack and person. Generated power from the coil is also calculated by taking the relative velocity of the backpack and the base and then multiplying that by the magnetic force.

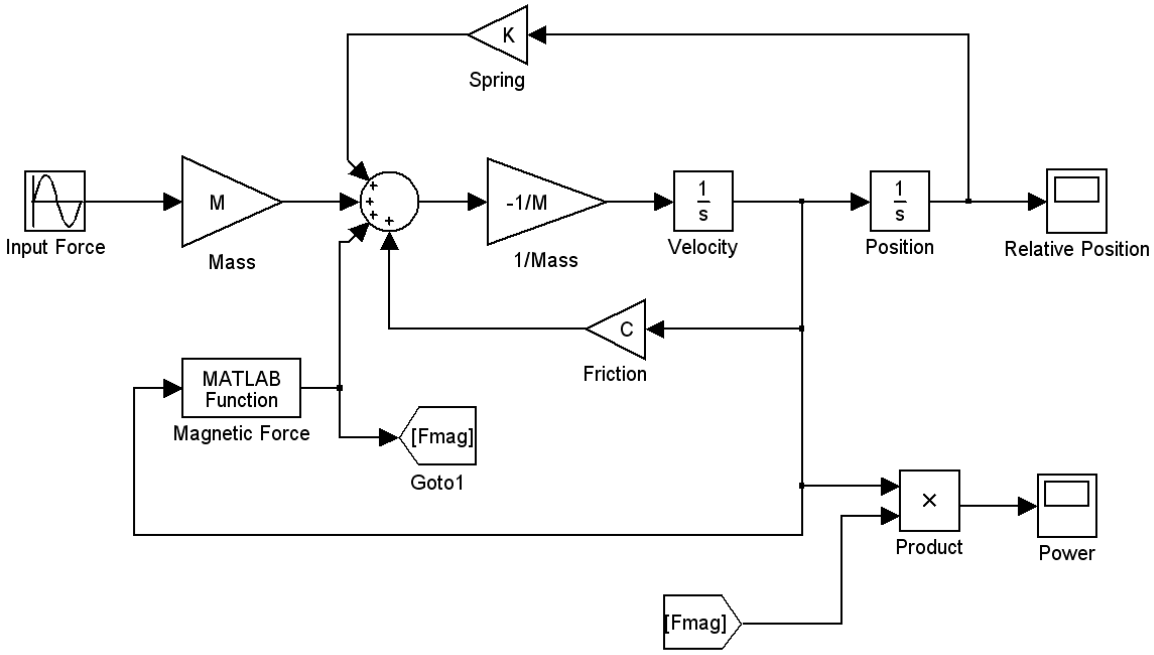

Figure 29. Simulink Block Diagram

The plot of magnetic force is shown in Figure 30, which shows the transient response and steady-state response. The steady-state response is similar to the result predicted by the magnetic model, as shown in Figure 24. This plot shows that the magnitude of the force is slightly less in the Simulink model, which is logical because the Simulink model includes friction and the magnetic model does not. The transient

response dies out quickly, which is what would be expected based on the particular solution of the differential equation used in the mechanical model. If the transient response did not die out quickly, the particular solution used in the mechanical model would not be valid. The transient response is not very large compared with the overall force extracted by induction. This shows that when the person begins walking, the backpack will not greatly affect the transmitted force on the wearer. If the transient response maximum force were too high, it would be hard for the person to overcome.

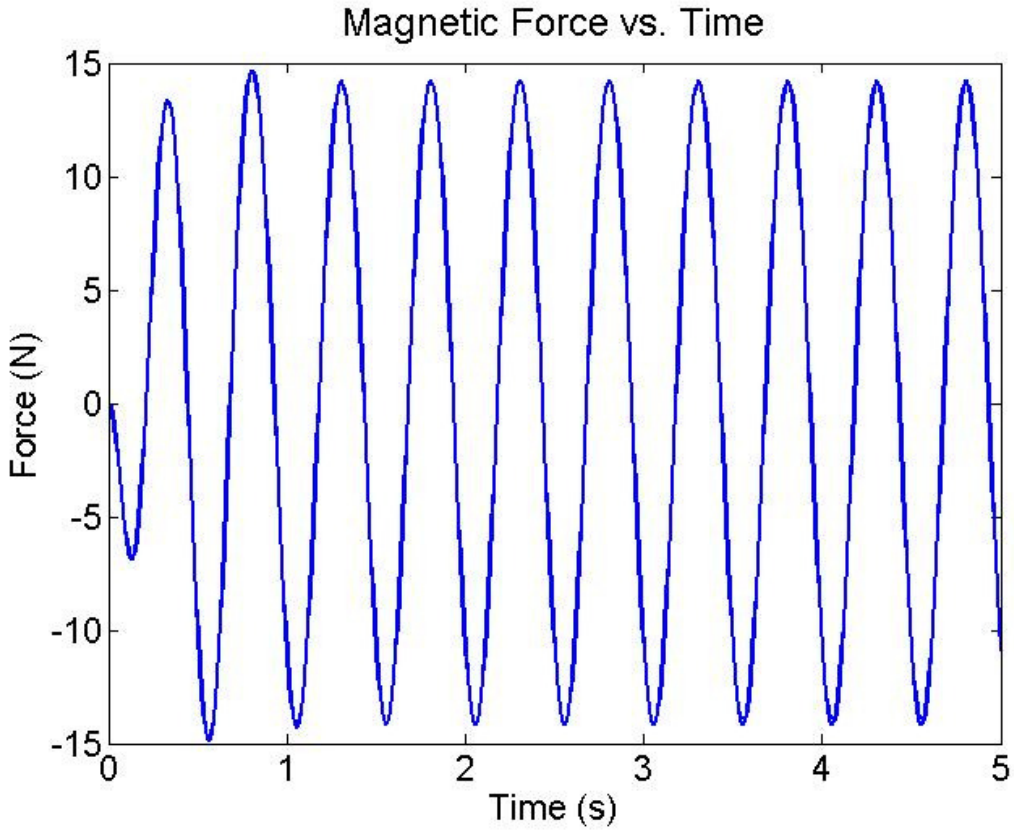

Figure 30. Simulink Magnetic Force

The power generated can be seen in Figure 31, which also shows the transient response dying out quickly. This generated power is also similar to the power predicted in the magnetic model, shown in Figure 25. The power increases with increasing magnet radius but the device is limited by the space available in the backpack frame. The increasing power from magnet radius is shown in Figure 32. The frequency is constant, but the amplitude of the power more than doubles when the radius is doubled.

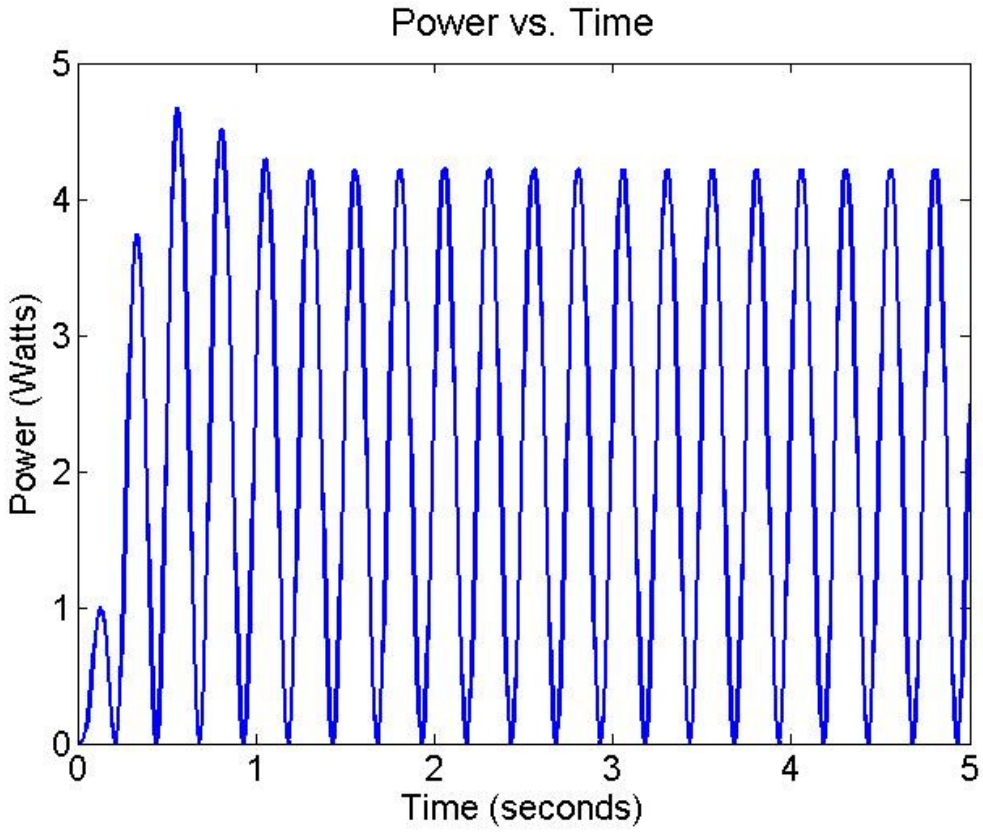

Figure 31. Simulink Predicted Power

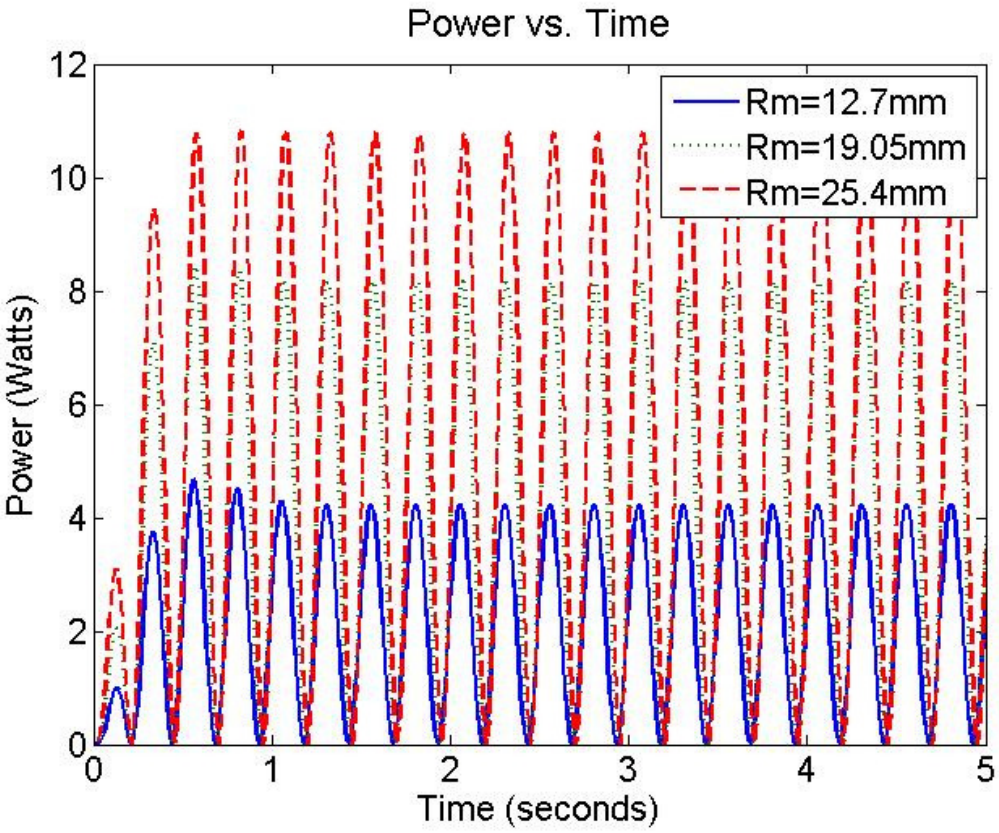

Figure 32. Power of Generator with Different Magnet Radii

The force and power are also peak calculation and the instantaneous force and power are shown in Figure 33 and Figure 34, respectively. The peak of the force and power represent the coil passing the steel spacer and dips are the coil passing the magnets.

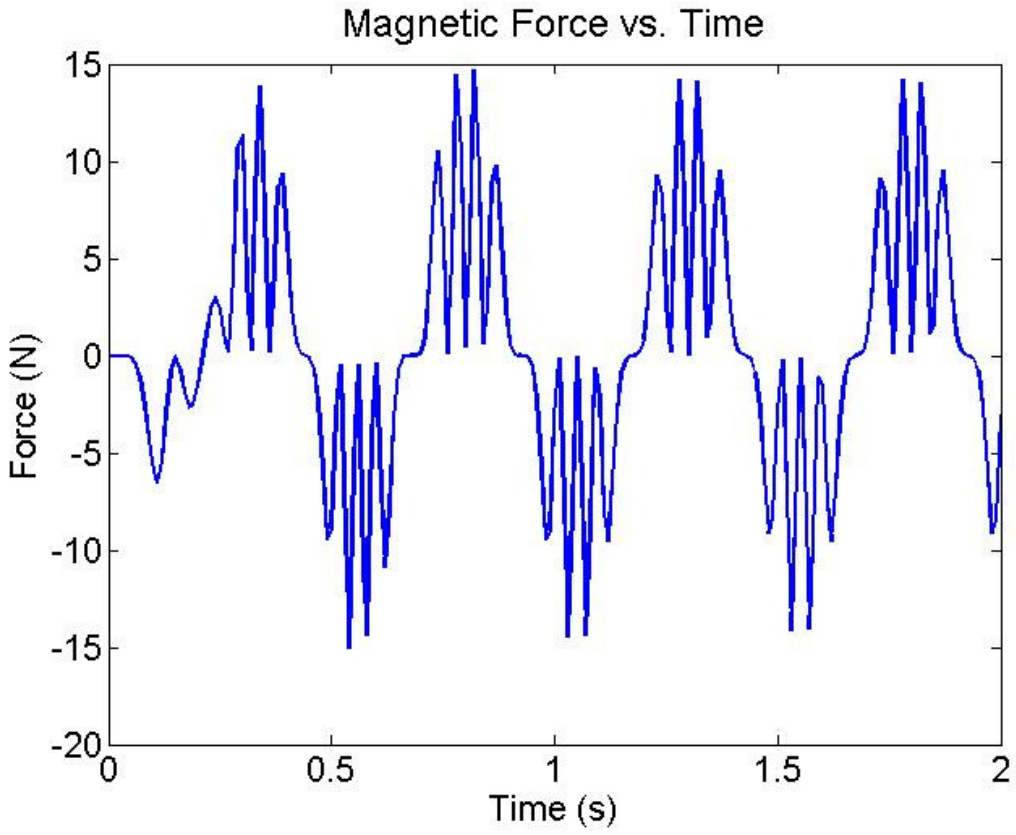

Figure 33. Magnetic Force Changing with Position and Time

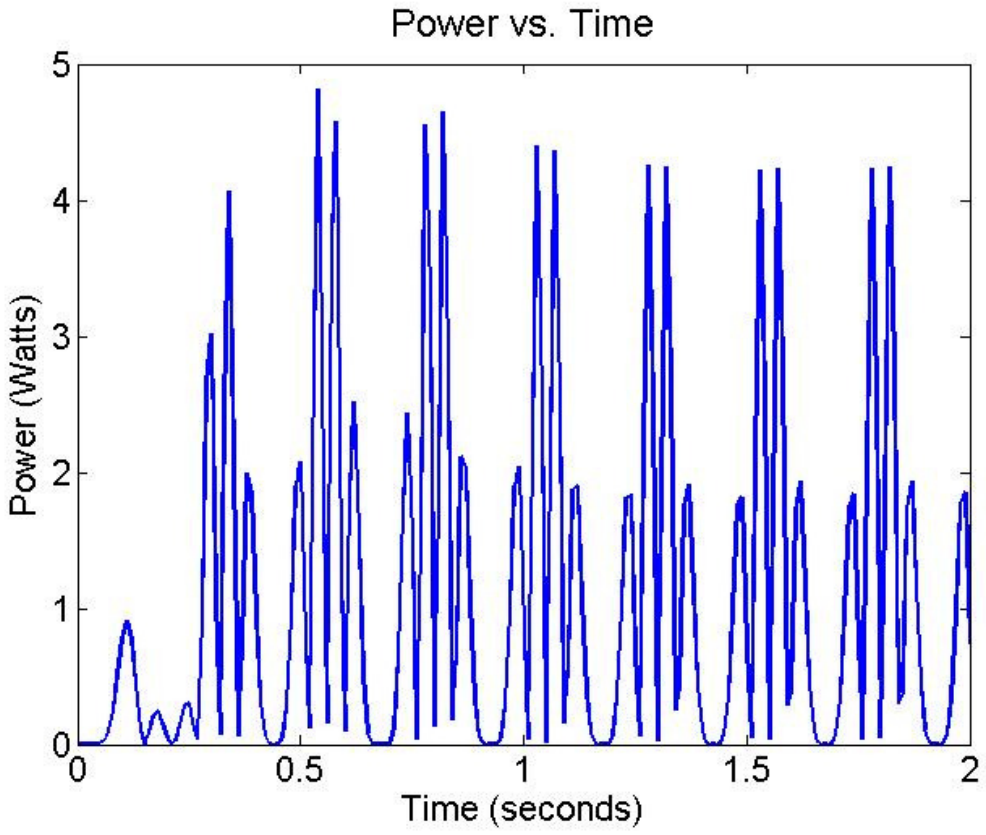

Figure 34. Power Changing with Position and Time

The Simulink model is a better predictor than the mechanical or magnetic model because it takes into account the transient response and solves the equation at each time step. It can also be used to calculate other useful information such as the Kinetic Energy of the system, shown in Figure 35.

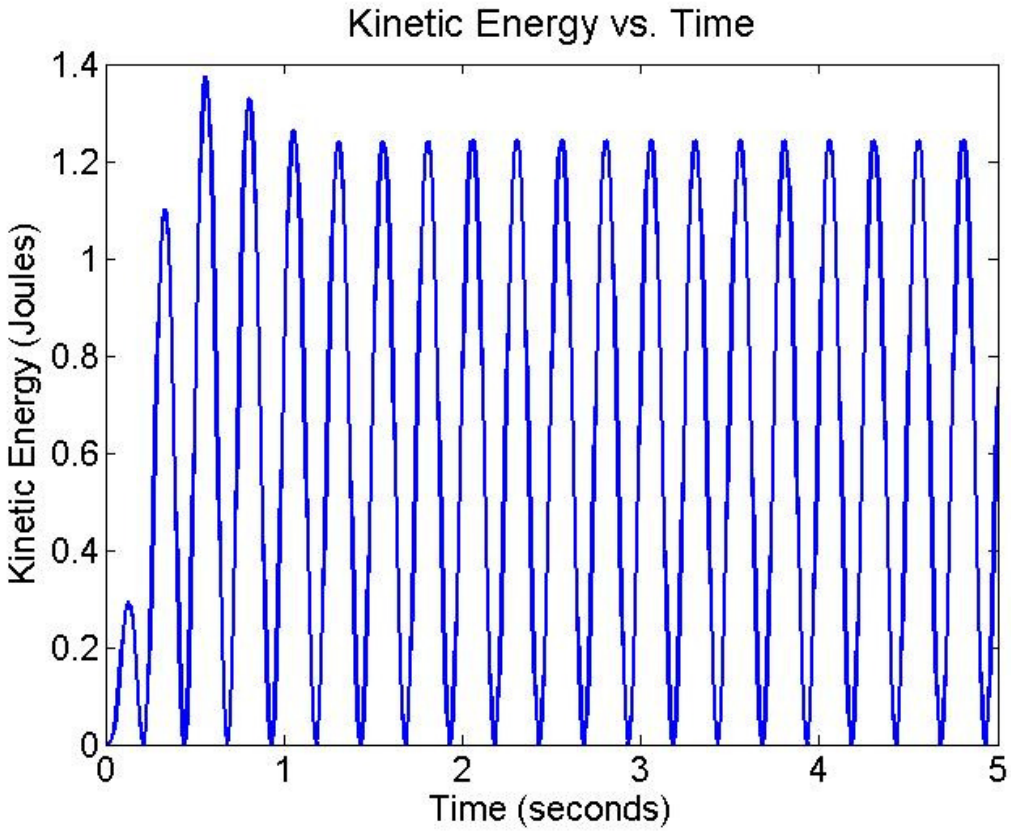

Figure 35. Kinetic Energy

DESIGN

The design of the electromagnetic generator is modeled after the tubular linear electrical generator device created by Baker [23] and from the analytical model developed in the previous section. The Mechanical, Magnetic, and Simulink models are used to determine the design requirements of the device. A summary of the requirements is shown in Table 1. The spring constant is based on the optimized frequency ratio observed in the Mechanical model. The backpack mass, amplitude, and walking frequency are base on values described by Rome et al. [14]. The outside diameter of the magnet is limited to one inch, similar to the backpack frame tube. From the Wang et al. [27] analytical model, the optimal spacer width, w_s, was found to be equal the magnet width, w_m, for the geometry chosen. The remaining values were determined by the Magnetic model to achieve the desired voltage. Fabrication of the generator was completed using the facilities in the C-MEMS Laboratory at Boise State University. The fabrication is discussed in detail in Appendix A.

Table 1 Geometry Summary Chart

Geometry	Symbol	Magnitude
Spring Constant	k (N/m)	8000
Mass	m (kg)	28
Amplitude of Person	Y (cm)	2.5
Walking Frequency	w (rad/s)	12.566
air gap	gap (mm)	0.4
Coil thickness	ch (mm)	5.2
Coil width	cw (mm)	12.7
Magnet Radius	Rm (mm)	12.7
Magnet width	wm (mm)	6.35
Spacer width	ws (mm)	6.35
Number of Coils	Nc	480

Electromagnetic Generator Design

The generator concept is shown in Figure 36. The armature is composed of a series of Neodymium magnets positioned axially. The magnets are shown in the figure as blue and red blocks. The red end is schematically the north magnetic pole and the blue is the south magnetic pole. The magnets are positioned with two north poles facing each other separated by a ferroelectric steel spacer. The south poles are also facing each other separated by another steel spacer. The coils are positioned cylindrically around the armature with a small air gap separating the inner coil from the magnets and spacers. This system is effective at various speeds and oscillation amplitudes. The magnets used were Neodymium ring magnets, axially magnetized, grade N52, with a nickel coating. The radius of the magnets is limited to 12.7 mm because of the diameter of a backpack

frame. An aluminum all-thread bar was used to align the magnets and steel spacers. The coils are fabricated using Low Temperature Co-Fired Ceramics (LTCC). To insure the current does not change direction between layers, the coils alternate direction between layers, shown in Figure 37.

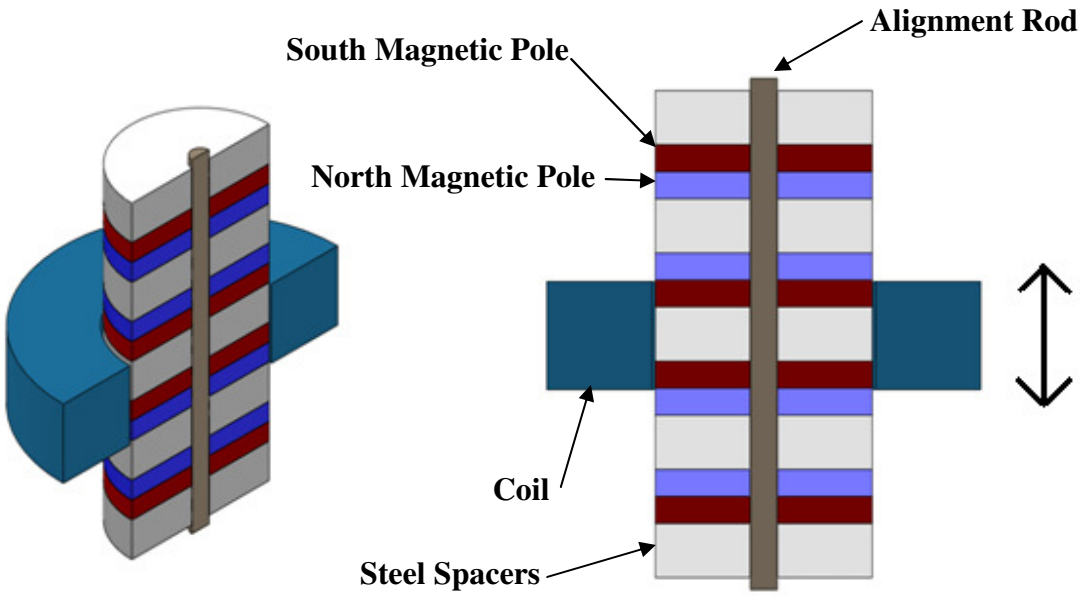

Figure 36. Linear Electromagnetic Generator Concept

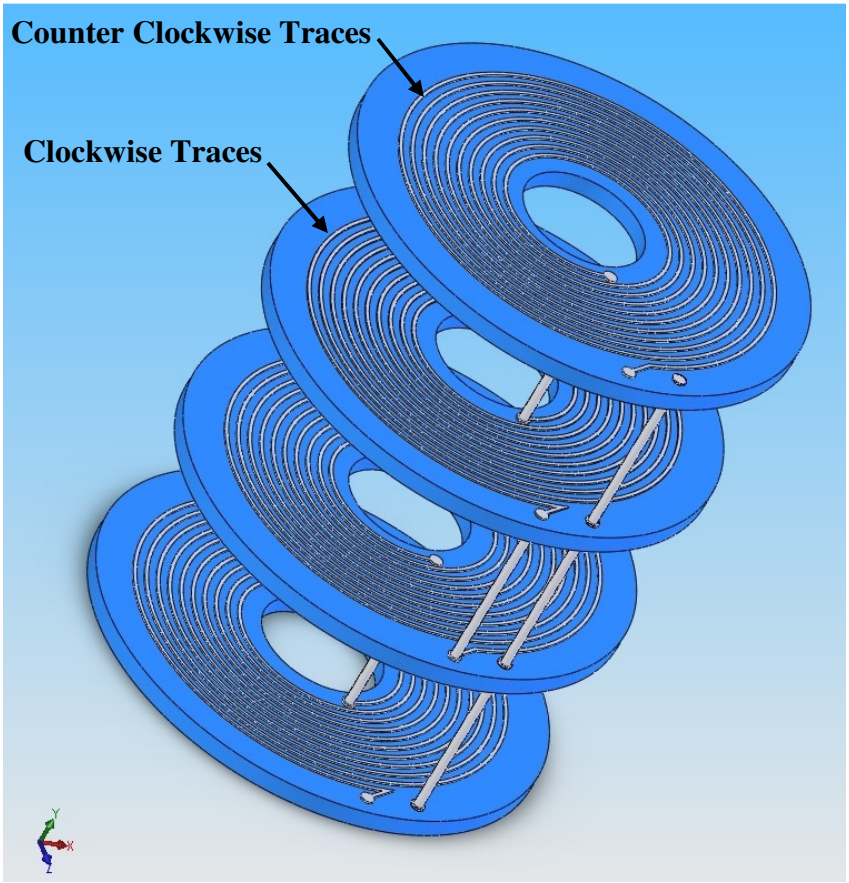

Figure 37. LTCC Coil Design

SUMMARY

A linear electromagnetic generator was studied to replace batteries for a soldier or backpacker. The mechanical system was modeled using the vibration of the movement of the backpack. The conservative energy produced by a person walking was used to predict the transmitted force the walker would experience while wearing the backpack. The transmitted force was reduced by decreasing the frequency ratio of the system. The available RMS power was also calculated in the mechanical model. A magnetic system was modeled after the work done by Baker [23] for an energy scavenging device used in ocean waves. The magnetic model uses information from the mechanical model to predict the generated power. A Simulink model was developed to combine the mechanical and magnetic model together and predict the power generated by the linear electromagnetic generator. The design of the generator was produced by input from the analytical model.

The power generated from the Magnetic and Simulink model is shown in Figure 38. In the start of the plot, the Simulink model is very different from the magnetic model, caused from the transient response in the Simulink model. As the transient response dies out, the two models have the same frequency with different amplitudes. There is slight time shift between the two models and this is caused by the time delay between models. The Simulink model includes friction in the equation of motion, which decreases the

power generated by the electromagnetic generator and the relative velocity is solved at each time step, adjusting the magnetic force. The magnetic model predicts a higher amount of power generated by the coil because it does not include friction in the calculations and does not adjust the relative velocity for the magnetic force slowing the system down.

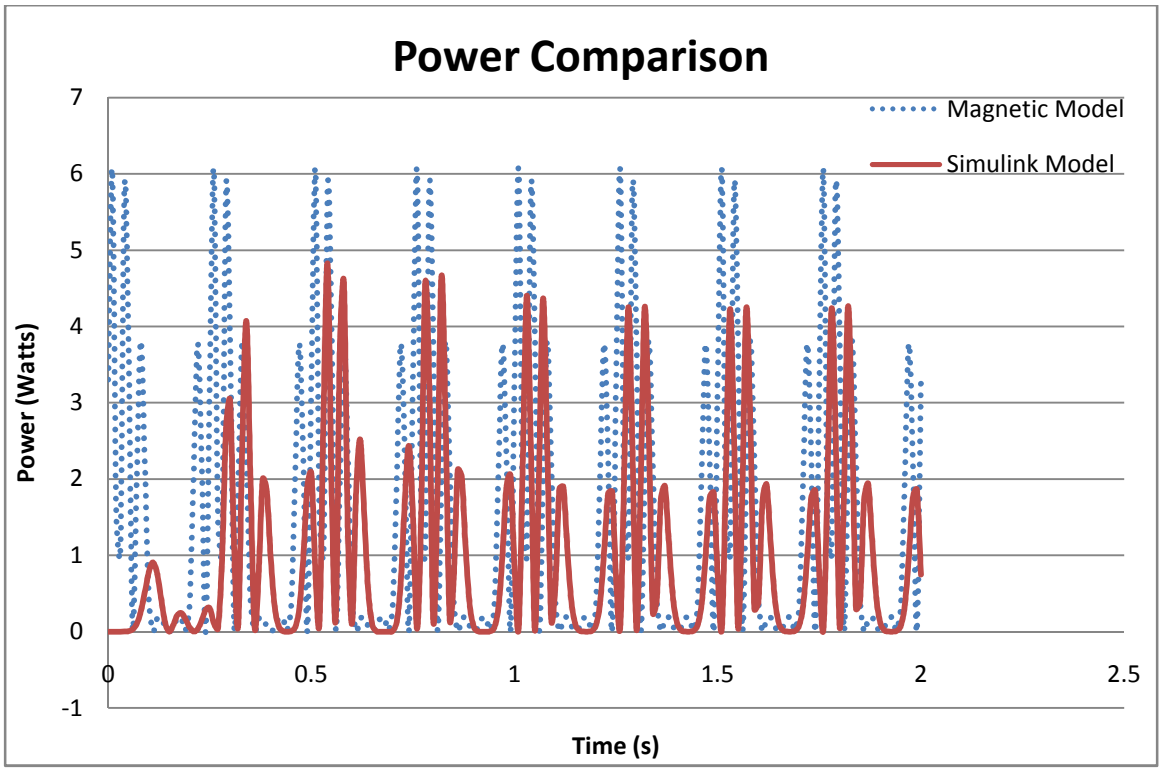

Figure 38. Power Comparison of Magnetic and Simulink Model

Future work will include optimizing the fabrication and design process to improve the experimental power output of the device. The backpack frame and power

storage will also be designed and integrated with the optimized energy scavenging system in future work.

LTCC is a potential fabrication option for inductive coils used in a portable power generation device. With optimization, the electromagnetic design could provide a useful source for portable power generation. The analytic model could be used for different magnetic configurations. Also, the linear electromagnetic energy scavenging device could be modified to work in other applications to generate power.

REFERENCES

[1] P. Patel-Predo. "Traveling light - micro fuel cells could give soldiers less weight to carry," *Spectrum, IEEE*, vol.43, no.7, pp. 20- 21, July 2006.

[2] J. Fjelstad and J. Murray. "Bringing wireless to the battlefield." *RF DESIGN,* vol. 24, pp. 48-57, 2001.

[3] D. Dunn-Rankin, E. Martins Leal, and D. C. Walther. "Personal power systems." *Progress in energy and combustion science,* vol. 31, pp. 422-465, 2005.

[4] S. F. J. Flipsen. "Power sources compared: the ultimate truth?." *Journal of Power Sources,* vol. 162, pp. 927-934, 2006.

[5] Committee on Electric Power for the Dismounted Soldier and National Research Council. (1997). *Energy-Efficient Technologies for the Dismounted Soldier.* [On-line]. Available: http://www.nap.edu/openbook.php?record_id=5905&page=R1. [September 27, 2011].

[6] K. C. Jiang, P. D. Prewett, M. C. L. Ward, Y. Tian, and H. Yang. "Design of a micro Wankel rotary engine for MEMS fabrication." SPIE Proceedings, MEMS Design, Fabrication, Characterization, and Packaging, Edinburgh, Scotland, 2001.

[7] N. S. Shenck and J. A. Paradiso. "Energy scavenging with shoe-mounted piezoelectrics." *Micro, IEEE,* vol. 21, pp. 30-42, 2001.

[8] M.J. Madou. *Fundamentals of Microfabrication: the Science of Miniaturization 2nd Edition.* Boca Raton, FL: CRC Press LLC, 2002, pp. 2,104.

[9] A. H. Epstein and S. D. Senturia. "Macro Power from Micro Machinery." *Science,* vol. 276, p. 1211, 1997.

[10] K. Peterson. "Novel Microsystem Applications with New Techniques in Low-Temperature Co-Fired Ceramics." *International Journal of Applied Ceramic Technology,* vol. 2, pp. 345-363, 2005.

[11] D.G. Plumlee. “Development of a Monopropellant Micro-Propulsion Device in Low Temperature Co-Fired Ceramics.” PhD dissertation, University of Idaho, Idaho, United States of America, 2007.

[12] DuPont. “951 Green Tape.” MCM951 datasheet, 2001.

[13] D.G. Plumlee, A. Moll, and J. Steciak. "Development of a Monopropellant Micro-Nozzle and Ion Mobility Spectrometer in LTCC." in *IMAPS Ceramic Initiative Workshop*, Denver, CO, 2004.

[14] L. C. Rome, L. Flynn, E. M. Goldman, and T. D. Yoo. "Generating Electricity While Walking with Loads." *American Association for the Advancement of Science, Science,* vol. 309, pp. 1725-1728, 2005.

[15] O. Danielsson. "Wave Energy Conversion: Linear Synchronous Permanent Magnet Generator." PhD dissertation, Uppsala University, Sweden, 2006.

[16] I. Ivanova, O. Ågren, H. Bernhoff, and M. Leijon. "Simulation of a 100 kW permanent magnet octagonal linear generator for ocean wave conversion," Fifth European wave energy conference, Cork, Ireland, pp. 17-19, 2003.

[17] O. Danielsson, E. Sjostedt, K. Thorburn, and M. Leijon, "Simulated Response of a Linear Generator Wave Energy Converter," ISOPE: Proceedings of the Fourteenth (2004) International Offshore and Polar Engineering Conference, Toulon, France, 2004.

[18] N. J. Baker, M. A. Mueller, and E. Spooner. "Permanent magnet air-cored tubular linear generator for marine energy converters," *Power Electronics, Machines and Drives, 2004. Second International Conference on (Conf. Publ. No. 498),* 2004, pp. 862-867.

[19] M. Mueller and N. J. Baker. "A low speed reciprocating permanent magnet generator for direct drive wave energy converters," *Power Electronics, Machines and Drives, 2002. International Conference on (Conf. Publ. No. 487),* 2002, pp. 468-473.

[20] J. Wang, W. Wang, G. W. Jewell, and D. Howe. "Design of a miniature permanent-magnet generator and energy storage system." *IEEE Transactions on Industrial Electronics,* vol. 52.5, pp. 1383-1390, 2005.

[21] J. Saunders, V.T. Inman, and H.D. Eberhart. “The major determinants in normal and pathological gait.” *Journal of Bone and Joint Surgery- American Volume*, vol. 35-A, pp. 543-558, July 1953.

[22] S.A. Gard, S.C. Miff, and A.D. Kuo. “Comparison of kinematic and kinetic methods for computing the vertical motion of the body center of mass during walking.” *Human Movement Science*, vol. 22, pp. 597-610, 2004.

[23] N. J. Baker. “Linear Generators for Direct Drive Marie Renewable Energy Converters.” PhD dissertation, University of Durham, England, United Kingdom, 2003.

[24] X. Xu, S. Hsiang, and G. Mirka. “An empirical validation of a base-excitation model to predict harvestable energy from a suspended-load backpack system.” *Theoretical Issues in Ergonomics Science,* vol. 11.6, pp. 546-560, 2010.

[25] D. J. Inman. *Engineering Vibration 3rd ed*. Upper Saddle River, New Jersey: Pearson Education, Inc., 2008, pp.130-132.

[26] R. D. Knight. *Physics for Scientists and Engineers Volume 4*. San Francisco, California: Pearson Education, Inc., 2004, pp.1041-1060.

[27] J. Wang, G. W. Jewel, and D. Howe. “A General Framework for the Analysis and Design of Tubular Linear Permanent Magnet Machines.” *IEEE Transaction on Magnetics,* vol. 35.3, pp. 1986-2000, 1999.

[28] M. Gongora-Rubio, L.M. Solá-Laguna, P.J. Moffett, J.J. Santiago-Avilés. “The utilization of low temperature co-fired ceramics (LTCC-ML) technology for meso-scale EMS, a simple thermistor based flow sensor.” *Sensors and Actuators A: Physical*, vol. 73.3, pp. 215-221, 30 March 1999

APPENDIX A

Fabrication

Fabrication

Fabrication started with 3D modeling software, SolidWorks, which was then split into parts representing the LTCC layers in 2D. CorelDRAW was used to create the LASER profile and screen printing pattern. DuPont 951PX LTCC sheets are 0.254 mm thick and have four sets of coils on each 90 mm x 90 mm substrate layer as seen in Figure A1. The features of each layer are milled using Universal M-300 LASER which is capable of cutting features as small as 0.1 mm. Cleaning and inspection of each layer after routing was required because of the particles accumulated during the milling process.

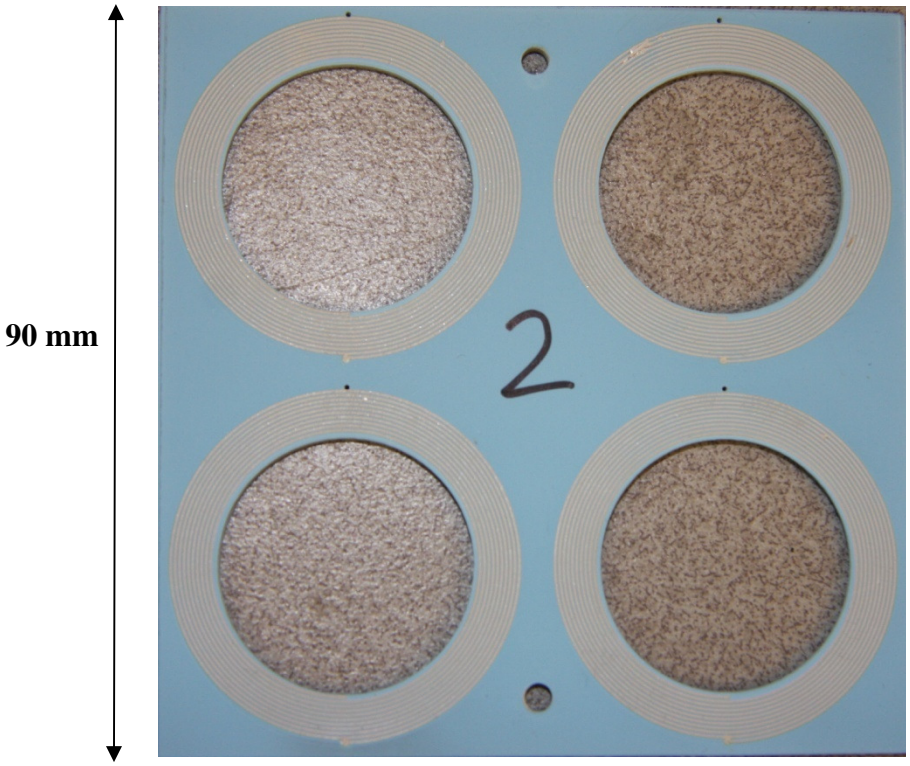

Figure A1. Four Sets of Coils Printed on DuPont 951PX

Vias were filled with DuPont 6141 silver conductive paste and are shown in Figure A2. A simple stencil and painting knife were used to fill each via. Each via was inspected to insure the hole is adequately filled with paste.

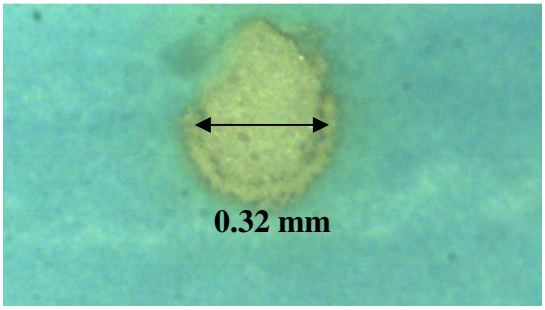

Figure A2. Via Filled with DuPont 6141 Silver Conductor Paste

Screens created by RIV, Figure A3, were used to apply the DuPont 6145 silver conductive paste onto the LTCC substrate to form the inductive coils. Some complications arose during this fabrication process. The traces were very closely inspected for breaks in the lines using a microscope. Breaks in the traces were created from small foreign particles trapped underneath the traces during printing. A commonly found particle was a small hair, shown in Figure A4. During firing the hair will burn away and leave a gap in the silver trace, thus breaking conductivity. This problem was overcome by using a Terra Universal Laminar Flow Bench 5' VLF and cleaning all work spaces before starting fabrication, as seen in Figure A5.

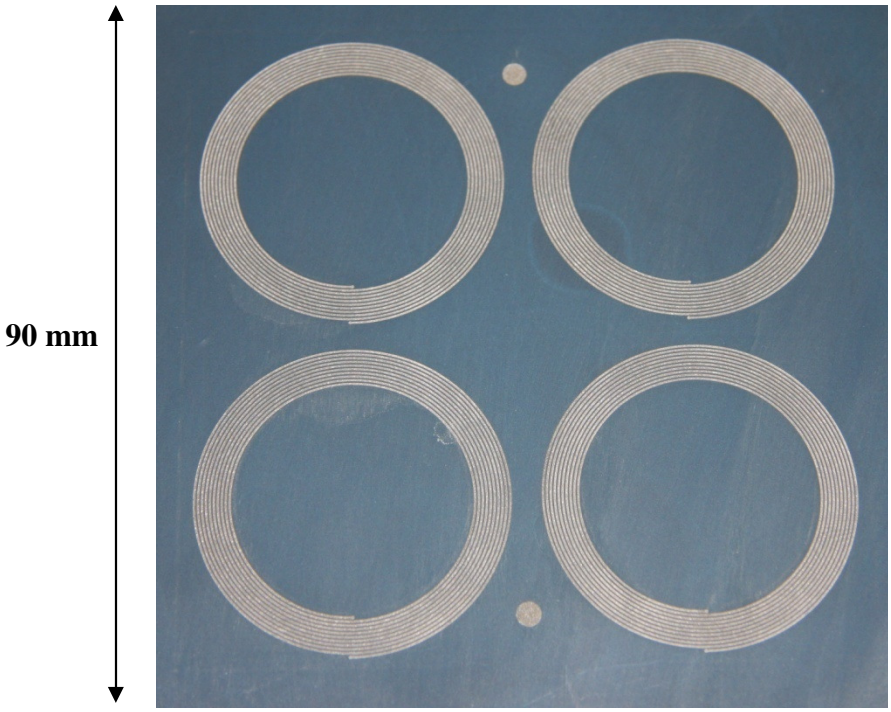

Figure A3. Screen of Silver Traces Made by RIV

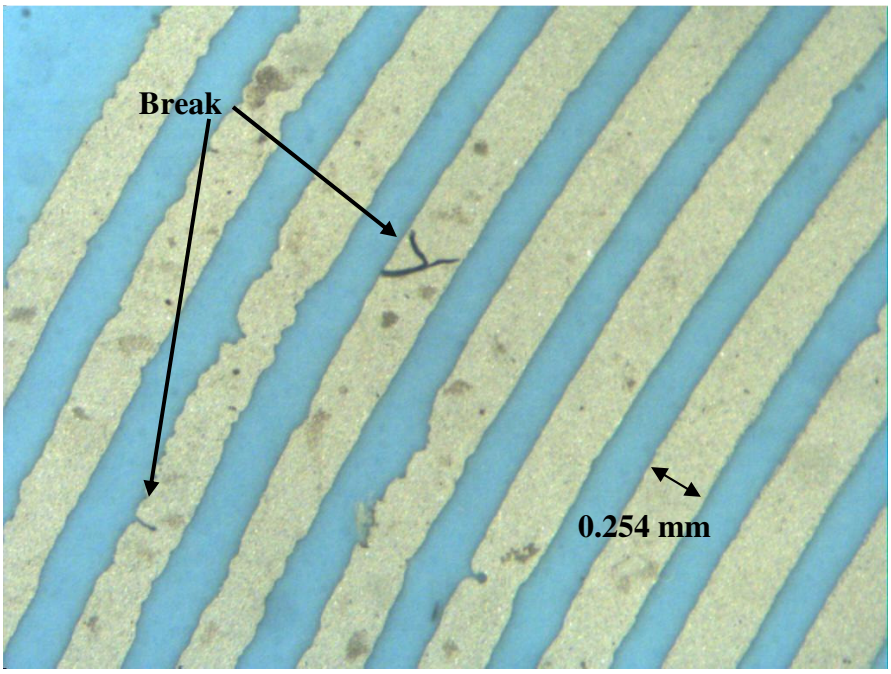

Figure A4. LTCC Silver Traces Showing a Break in the Trace

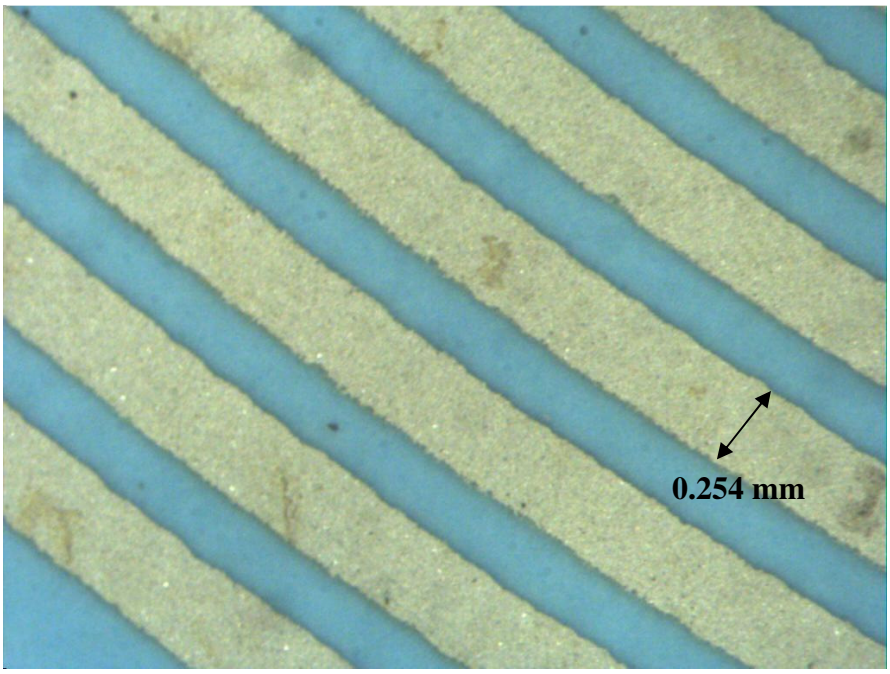

Figure A5. LTCC Silver Trace Improved

The ceramic layers are collated, stacked 6 layers high and pressed in a PHI Thermal Uni-axial Hydraulic press heated at 70°C and pressed at 20.68 MPa for 10 minutes. The coils are then milled out of the 90 mm x 90 mm squares into a round shape using the LASER. They are collated, stacked, and bonded together using Poly-2-ethyloxazoline (PEOX). A second lamination is required to bond the rounded coils, but the uni-axial press compressed and collapsed the first attempt, shown in Figure A6. A different approach was needed due to the high layer count and the circular shape of the coils. The KEKO Isostatic Laminator was used to laminate all of the layers together resulting in a device that is 48 layers tall with 10 coils per layer and a total of 480 coils.

Figure A6. First Coil Prototype Compressed by the Uni-Axial Press

After lamination the coils are fired in a Lindberg/Blue Box Furnace with a firing profile shown in Figure A7. The furnace is programmed to ramp up to 365°C and burn the organic binder. The furnace then ramps to 850°C for sintering of the LTCC. Liquid phase sintering shrinks the device 12% in the x and y directions and 15% in the z direction documented by Gongora-Rubio [28]. The final product is a hermetically sealed device with 480 coils and only 12.7 mm tall, shown in Figure A8.

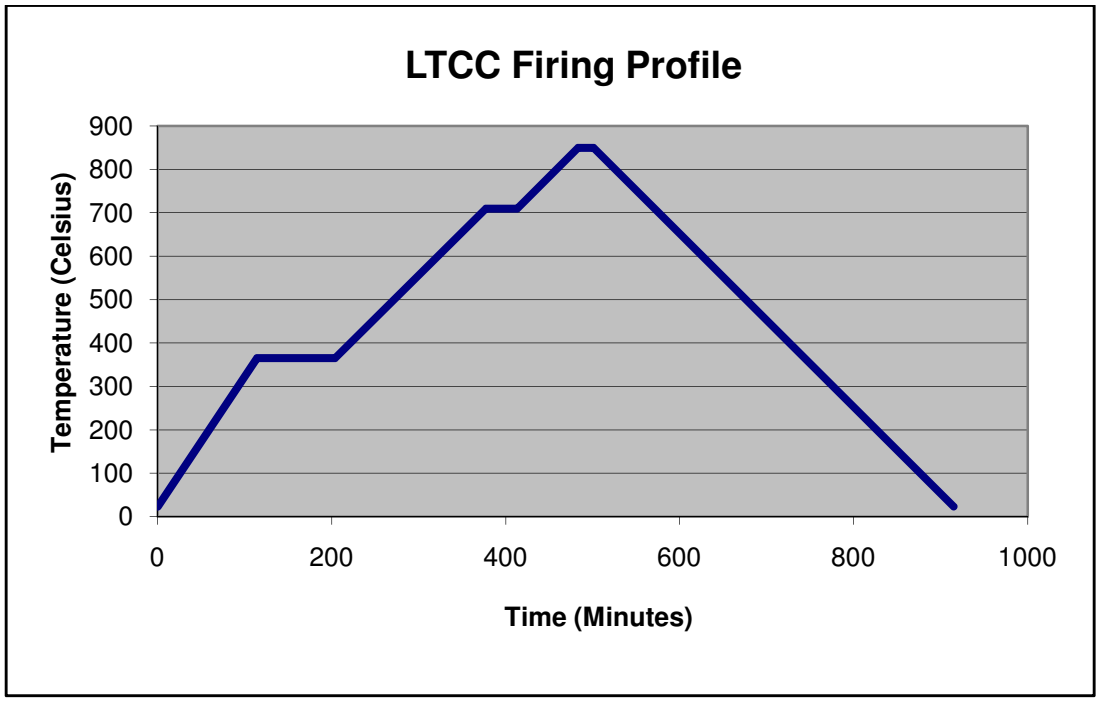

Figure A7. LTCC Firing Profile

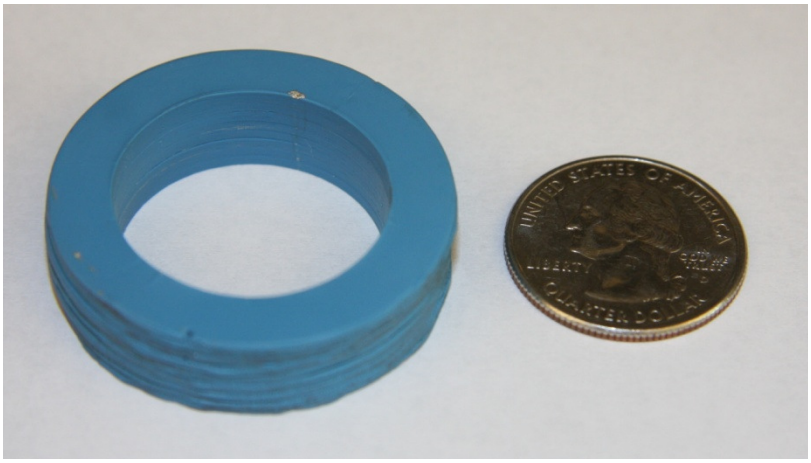

Figure A8. Induction Coils in LTCC

APPENDIX B

MATLAB Script File for the Magnetic Force

MATLAB Script File for the Magnetic Force

```
function Fm = Fmag1(u)

%Inputs
%u(1)= relative position
%u(2)= relative velocity
v = u(2);
x = u(1);

%Constants
gap = 0.0002;                                   %Air gap (m)
ch = 0.0052;                                    %Coil thickness (m)
Rm = 0.0127;                                    %Magnet Radius (m)
wm = 0.00635;                                   %Magnet Width (m)
Wp = 2*wm;                                      %Pitch of Rotor(m)
ws = wm;                                        %Steel Spacer Width (m)
mur = .99998;                                   %Permeability
cw = Wp;                                        %Coil Width (m)
lg = Wp/pi;                                     %Effective Air Gap
Br = 1.5;                                       %Remanent Flux Density (T)
Bg = (pi*Br*Rm*wm)/(2*mur*Rm*Wp+pi*wm*ws);      %Flux Density at Rotor (T)
Ro = Rm + gap +ch;                              %Outer Radius of coil (m)
Ri = Rm + gap;                                  %Inner Radius of coil (m)
vol = pi*cw*(Ro^2-Ri^2);                        %Volume of Coil (m)
ra = (Ri + Ro)/2;                               %Average Radius of coil (m)
Ncoil = 480;                                    %Number of Coils
Ndevices = 1;                                   %Number of Devices
Lp = Ndevices*Ncoil*2*pi*ra;                    %Path length of coil
Rsis = 10;                                      %Resistance of Coil (ohms)

%Calculate flux density along rotor (T)
if 0 < x && x < Wp
    Ba = Bg*sin(pi*x/Wp);
elseif Wp < x && x < 2*Wp
    Ba = -Bg*sin(pi*x/Wp);
elseif 2*Wp < x && x < 3*Wp
    Ba = Bg*sin(pi*x/Wp);
elseif -Wp < x && x < 0;
    Ba = -Bg*sin(pi*x/Wp);
elseif -2*Wp < x && x < -Wp;
    Ba = Bg*sin(pi*x/Wp);
elseif -3*Wp < x && x < -2*Wp;
    Ba = -Bg*sin(pi*x/Wp);
else
    Ba = 0;
end
```

```
%magnetic force (N)
Fm = (cw*pi*v*Lp^2*Ba^2*lg*exp(-2*gap/lg)*(2*Ri+lg-(2*Ro+lg)*exp(-
2*ch/lg)))/(2*Rsis*vol);
```